Modern Electronic Materials 3 (2017) 1–25

Contents lists available at ScienceDirect

Modern Electronic Materials

journal homepage: www.elsevier.com/locate/moem

Current state and perspectives for organo-halide perovskite solar cells. Part 1. Crystal structures and thin film formation, morphology, processing, degradation, stability improvement by carbon nanotubes. A review☆

Nigmat Ashurov[a], Boris L. Oksengendler[a], Sergey Maksimov[a], Sayyora Rashiodva[a], Artur R. Ishteev[b,*], Danila S. Saranin[b], Igor N. Burmistrov[b], Denis V. Kuznetsov[b], Anvar A. Zakhisov[b,c]

[a] *Science Centre of Chemistry and Physics of Polymers, National University of Uzbekistan named after Mirzo Ulugbek, 7b A. Kadyri Str., Tashkent 100128, Uzbekistan*
[b] *Energy Efficiency Center, National University of Science and Technology MISiS, 4 Leninskiy Prospekt, Moscow 119049, Russia*
[c] *Department of Physics, University of Texas at Dallas, 800 West Campbell Road, Richardson, TX 75080-3021, USA*

ARTICLE INFO

Keywords:
Perovskite
Solar cell
Photovoltaic
Organic photovoltaic
Stability
Thin film
Carbon
Carbon nanotubes
Graphene
Polymer
Nanoimprint

ABSTRACT

The fundamental problems of the modern state of the studies of organic–inorganic organo-halide perovskites (OHP) as basis for high efficiency thin film solar cells are discussed. Perovskite varieties and background properties are introduced. The chronology of development of the studies in this direction has been presented – structural aspects of these OHP perovskites, from early 2D to recent 3D $MAPbI_3$ perovskites and important technological aspects of smooth thin film structure creation by various techniques, such as solvent engineering, spin- and dip - coating, vacuum deposition, cation exchange approach, nanoimprinting (particularly, a many-sided role of polymers). The most important theoretical problems such as electronic structure of lattice, impurity and defect states in pure and mixed perovskites, suppressed electron-hole recombination, extra-long lifetimes, and diffusion lengths are analyzed. Degradation effects associated with moisture and photo irradiation, as well as degradation of metallic electrodes to OHP solar cells have been considered. The application of carbon nanostructures: carbon nanotubes (CNT) and graphene as stable semitransparent charge collectors to OHP perovskites is demonstrated on the example of original results of authors.

1. Introduction

Global energy crisis and environment pollution become threatening factors for human being evolution. Addressing these problems is in the field of development of effective alternative renewable sources of energy. Undoubtedly, among a variety of such natural sources a leading place is occupied by solar radiation.

Unlike the traditional sources such as coal and fuel, the sun is a reliable steady and stable source of energy. The traditional solar cells on the basis of silicon and other combinations of inorganic semiconductors provide conversion up to 30%, but their wide application is restricted by high cost.

The photovoltaic devices (PD) converting solar energy into electric one are a base of many compositions and technologies of solar cell creation.

Therefore, development of new efficient technologies of PD is of great interest for industry.

A list of alternative and very promising PD technologies having low cost contains organic photovoltaics (OPV), solar cells with dyes (DSSCs) as absorbers and thin-film technologies.

The absorber efficiency is defined by a width of the interval of absorbing the wave lengths of solar radiation (350–950 nm) and a completeness of the conversion of incident light on charges.

The thin-film solar cells are significantly cheaper, as compared to highly crystalline silicon, owing to low cost of initial components and production process. At the same time, the production of classical cells based on thin-film Si and inorganic compound semiconductors requires vacuum and high temperature, which inevitably leads to higher cost. The organic photovoltaic cells are technological in production. However, owing to fundamental energy losses in the process of charge dissociation on bulk hetero-transitions they have less conversion than the silicon cells.

☆Peer review under responsibility of the National University of Science and Technology MISiS.

* Corresponding author.
E-mail address: arturishteev@misis.ru (A.R. Ishteev).

http://dx.doi.org/10.1016/j.moem.2017.05.001
Received 10 December 2016; Accepted 29 March 2017

2. Chronology of development of solar cells based on perovskite

The perovskites with the general formula ABX_3, analogs of natural mineral $CaTiO_3$, were discovered by Weber in 1987; their structure and properties were studied in detail by Mitzu et al. [1–5] when they created field transistors and light diodes. The total characteristics of the ABX_3 compounds were given by the Stoumpos group [6]. Semiconductor perovskite **(SP)** is a special class of the materials meeting all the requirements for solar radiation adsorbers, namely direct-zone with the high coefficient of absorption and charge mobility [5,7]. Perovskites are very technological for formation of corresponding layers through a solution on different substrates. The beginning of perovskite application is connected with solar cells on the basis of dyes. The first solar cell based on perovskite $CH_3NH_3PbBr_3$ with I^-/I_3^- electrolyte with conversion 2.19% was created by Miyasaka et al. in 2006 [8]. Afterwards, modifying mesoporous titanium oxide and electrolyte nature, the same group could get conversion 3.13% and 3.81% for perovskites $CH_3NH_3PbBr_3$ and $CH_3NH_3PbI_3$, respectively [9]. It was remarkable that for perovskite bromide the voltage of open circuit (V_{oc}) was about 1 V. However, the authors noted that owing to perovskite solving in acetonitrile the cells stopped to operate. Substitution of acetonitrile with a nonpolar solvent – ethylacetate [10] allowed conversion 6.2% (much higher than for dye No. 719 – 3.89%). However, in this case and for the same reason the cells lost their 80% efficiency for 10 min. It should be noted that because of the dimensional dependence of opto-electric characteristics the authors attributed the created cell architecture to a class of the cells sensibilized with quantum dots (QD) as such was, in this case, $CH_3NH_3PbI_3$. The use of QD (CdS, CdSe, PbS, PbSe, InP, InAs, Sb_2S_3) as absorbers instead of dyes was the most significant stage in solar cell development [9–15].

In spite of the good photovoltaic parameters the cells on the basis of quantum dots are instable. They have low V_{oc} and rapid recombination of charges, which impedes to achieve the high conversion efficiency.

The problem of perovskite solubility in liquid electrolyte was solved by Kim et al. [16] by electrolyte replacement with a hole-transport semiconductor spiro-OMeTAD (2,2′,7,7′ – tetrakis (N, N-di-p-methoxypheniamine) – 9,9' – spirobifluorene). The conversion was 9.7% with operability at the level of this conversion for approximately 500 h. By photoinduced absorption spectroscopy the authors found two processes – injection of holes from perovskite to spiro-OMeTAD and electrons to mesoporous TiO_2.

A little bit later but in the same year, Etgar et al. [17] demonstrated that the nano-particles of perovskite iodide can be simultaneously an absorber and a conductor of holes. For a cell without hole transporter with the use of titanium oxide nano-plates exposed in plane 001 the conversion was obtained 5.5% for standard power of solar simulator AM 1.5 1000 Wt/m^2 and 7.3% for lower intensity 100 Wt/m^2. In another work at the same time, using a thin-film technology, Lee [18] showed that mixed perovskite $CH_3NH_3PbI_2Cl$ has simultaneously the properties of a nice absorber and conductor of electrons. Using spiro-OMeTAD as a hole transporter and mesoporous Al_2O_3 (an insulator with the band gap 7–9 eV) instead of titanium oxide the authors obtained conversion 10.9% (8% with titanium oxide). The cells with such construction were called as mesosuperstructured ones. In a number of the key aspects of development of this direction an experimental fact should be noted. This fact was found by Snaith et al. [19] when they measured the diffusion lengths of electrons and holes for the planar configuration of cells (p–i–n structure) on the basis of perovskite iodide and chlorine-doped perovskites. These values are sufficiently balanced and averaged about 100 nm and over 1000 nm, respectively. Despite the fact that the reasons for such a behavior have not been revealed until now these results were used to select architecture of the cells with iodine and mixed perovskite. Namely, for $CH_3NH_3PbI_2$ a mesoporous configuration of the cell is acceptable and for $CH_3NH_3PbI_{3-x}Cl_x$ a planar one is quite acceptable. From the practical point of view the latter is more preferable owing to manufacturability. In a series of the subsequent works published in 2013–2015 almost everybody noted how it is important to make a highly qualitative film of perovskite with a maximal degree of crystallinity and covering of a corresponding substrate (mesoporous or dense metal oxides). Addressing those problems became a base for so rapid strengthening of the power conversion efficiency of the perovskite-based cells. Detailed consideration of this problem is mainly connected with a non-controlled development of the morphology in the process of perovskite film formation. The group Grätzel [20,21] realized a sequential deposition of the precursors of perovskite iodide, namely at first a film is formed from the PbI_2 solution on a mesoporous substrate and then it is dipped in the solution of methylammonium iodide. As a result of the proposed method, the cells with high reproducibility and conversion ~15% were obtained. Developing the ideas on optimization of conditions of perovskite film formation, Snaith et al. [22] realized a vacuum deposition of the precursors $CH_3NH_3PbI_{3-x}Cl_x$ in the planar configuration of the cell and achieved the conversion ~15.4%.

Taking into account that the vacuum deposition is a complicated technological process, Chen [23] proposed a similar technology [20] differed by the second stage: instead of dipping, the lead iodide film moves through vapors of methylammonium iodide. The kinetically favorable conditions of the precursor interaction lead to formation of a qualitative film of perovskite with an optimal coverage of the dense titanium oxide in the planar configuration of the cell on the basis of perovskite iodide. As a result, the best conversion efficiency exceeding 12% was obtained for this perovskite. A three-step technology [24] of producing a perovskite film deserves attention. This technology allows excluding a film of non-reacted PbI_2.

Great attention was paid by the researchers to selection and modification of materials with electron and hole transportation. Modification of dense titanium oxide in the planar configuration of cells with small amounts of graphene [25] and titanium diisopropoxide bis (acetilacetonate) [26] to decrease series resistance allowed for mixed perovskite the conversion efficiency 15.6% and 15.9%, respectively. Coordination of the energy levels of the hole-transport component (poly – triarylamine – PTAA) [27,28] and spiro – OMeTAD [29] and optimization of series resistance allowed strengthening the conversion efficiency from 16% to 19.3% [30].

The rapid growth of publications for recent years and conversion efficiency (Fig. 1) of the cells on the basis of perovskites as compared to alternative approaches is evidence of reasonable forecasts [31] of about the 25% conversion. There is every reason to hope that in the nearest time this value will be comparable with that of the cells on the basis of crystalline silicon.

The unusually fast steady growth of performance of perovskite photovoltaic cells is based on new exciting physics processes, which are found in 3-D perovskite semiconductors. Although many of them are not yet well understood, we need to outline here the most important and unusual features of perovskite electronic and optical properties, which have been found by different groups [32–34].

Impressive power conversion efficiency of solar cells based on hybrid lead halide perovskites reported in recent years still awaits a solid understanding of its microscopic origin. So photocarrier density and intrinsic Hall mobility, directly obtained in these materials in steady-state transport measurements, unambiguously demonstrate that both electron-hole recombination and charge trapping processes are suppressed. Electron-hole recombination coefficient explicitly measured in experiments ([35] on Hall Effect) (10^{-11}–10^{-1} $cm^3\ s^{-1}$) is on par with some of the lowest coefficients in high-purity single crystals of direct-band inorganic semiconductors. Such as GaAs. Steady-state carrier lifetimes (up to ~3 ms) and diffusion lengths

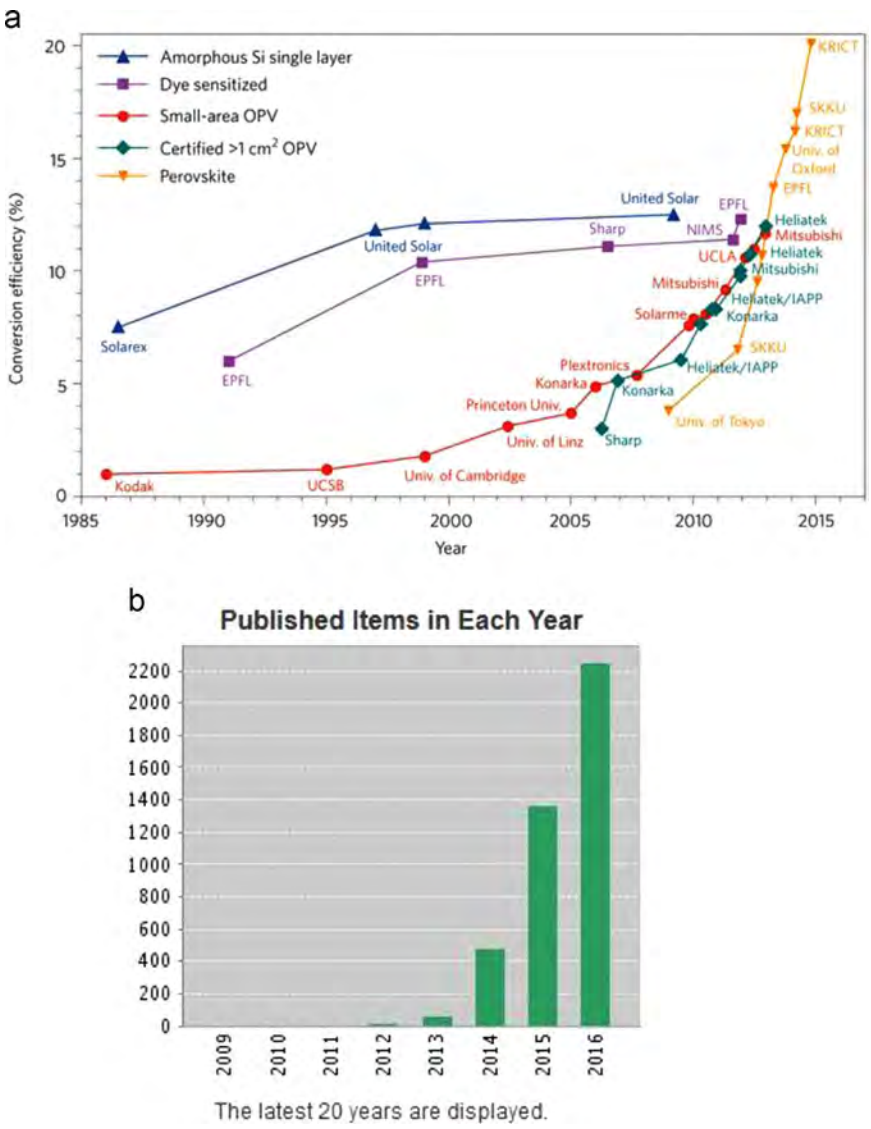

Fig. 1. (a) Efficiency records vs. year of third generation (emerging) PVs. The orange line indicates that the efficiency of PSCs has improved dramatically. Reprinted with permission from [32] (b) The number of publications "perovskite solar cell" according to WOS.

(as long as ~650 μm), directly obtained in electrical transport measurements, show that these parameters are much longer in these solution or vapor processed hybrid materials than in the best available direct-gap inorganic semiconductors, which is truly amazing, if one keeps in mind the "easy and low temperature" solution processing of this films [36]. Our results clearly suggest that a relatively slow charge carrier transport with the intrinsic single-crystal Hall mobilities of up to ~ 60 $cm^2 V^{-1} s^{-1}$ and a suppressed *e-h* recombination are of intrinsic origin. It was suggested that one type of explanation for this effects is due to a new type of polaron, formed by rotation of organic methylammonium dipoles surrounding charge carriers, charged impurities or traps can explain the observed behavior. This polaronic effect may not only decrease the charge carrier mobility, but also significantly reduce the Coulomb capture cross section and trapping rate in hybrid perovskites [37]. An effective repulsion between the polaronic dresses of oppositely charged polarons (via the short-range polarization field interference effects) can further suppress recombination. Another possible explanation of mentioned effects is related with a "protected" nature of carriers in hybrid perovskites, due to which the carriers are protected from scattering, from recombination, from trapping. The origin of this "protection" is still under intense discussions [38,39].

3. Structural aspects of organo-halide perovskites

3.1. 2-D provskite

Perovskites materials were named by Gustav Rose in 1839 in honor of Count Lev Alekseevich Perovski. The 1-st paper about the lead halide perovskites in 1892 was presented by Welles [40]. The halide (Cl, Br, I) perovskites based on Cs and Pb were described.

Initially organic–inorganic perovskites have received considerable attention due to their unique structures of organic and inorganic alternating layers. But the most attention perovskites paid because of properties, especially optoelectronic properties, such as a large absorption coefficients, high charge carrier mobilities, and long exciton diffusion length.

Early publications on lead halide organic-inorganic perovskites were presented by D. Weber in 1978 [41,42], they were about Sn and Pb based perovskites with CH_3NH_3X (X = Cl, Br, I) organic part.

Historically the 2-D perovskites with the schematic structure shown at Fig. 2 have been studied very actively, particularly by David Mitzi and co-workers [2–4,43,44]. The layer perovskites are typical "sandwich" systems; in fact their structure results from the regular alternation of inorganic and hydrocarbon regions, so that

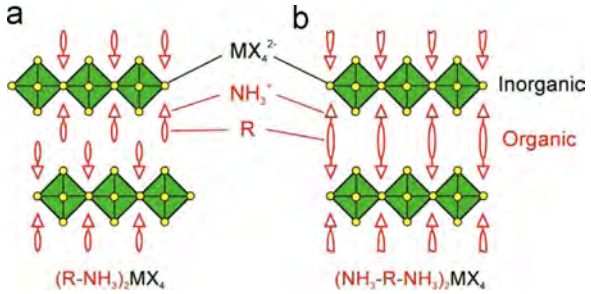

Fig. 2. Schematic representation of single-layer (n=1) < 100 > -oriented perovskites with (a) monoammonium ($R\text{-}NH_3^+$) or (b) diammonium($NH_3^+\text{-}R\text{-}NH_3^+$) organic cations [45].

each inorganic layer is sandwiched between two hydrocarbon layers and vice versa.

The organic component of the sandwich structures may consist of a bilayer or monolayer (for diammonium) of organic cations (Fig. 2a). Bilayer structure form, if cations are monofunctional (for exemple - monoammonium), in that case the ammonium head of the cation of hydrogen/ionically bonds to the halogens in one inorganic layer, and the organic group extends into the space between the inorganic layers [45,46]. For bifunctional (diammonium cations) organic cations (Fig. 2b) between inorganic layer placed organic monolayer with located on each side functional (for exemple - ammonium) groups; therefore, no van der Waals gap exists between the layers.

Inorganic layers are conceptually derived from the three-dimensional AMX_3 perovskite structure, if they are cut along one of the crystal lattice directions [45] (Figs. 3–5).

The nature of *A* cations is previously depending directions of the crystal lattice cutting. In the general formula (AMX_3) *A* cations are usually metal ions such as calcium, potassium, sodium, strontium, lead, cerium (or various rare metals), etc. in conventional perovskites.

In an organic–inorganic hybrid perovskite, *A* is replaced by organic cations [45]. Because of the space limitation, only the small organic cations can be integrated into the 3D perovskite. Generally the organic cations consist of three or less C–C or C–N bonds. The most common examples are methylammonium or the larger formamidinium.

It was shown that small $[CH_3NH_2]HI$ cations occupied the vacancies of the polyoctahedron PbI_2 and the longer $[C_4H_9NH_2]HI$ cations lie on the both side of the perovskite slabs in a self-assembling process. Although there is no clear investigation of how the molecules stack into the layered structure, it is believed that the driving forces for the molecules self-assembling including [46]: (a) the inorganic ions prefer to form the extended octahedral network by ionic bond; (b) organic molecules hydrogen/ion bond with inorganic perovskite sheets on both sides; (c) the organic R group interdigitate between the inorganic sheets by van der Waals interaction.

The layer perovskites systems can be from, if the 3D perovskite crystal cut along three one of three directions: < 100 >, < 110 > or < 111 > [45] (Fig. 3).

The < 110 > -oriented perovskite sheets are conceptually derived from the 3D AMX3 and cut along the < 110 > direction (Fig. 4). These perovskites can be stabilized by the cooperation of methylammonium and iodoformamidinium cations or the latter themselves [2,47]. In above example, the iodoformamidinium cations play an important role of directing the selfassembling of special < 110 > -oriented perovskites.

The < 110 > -oriented perovskites have been formed also in the absence of iodoformamidinium cation, in work [46] was develop a route to fabricate < 110 > -oriented perovskite using only one class of cation: N-(3-aminopropyl)imidazole [46] or 2-(aminoethyl)isothiourea [48].

The < 111 > -orientated layered perovskites (Fig. 5) are more rarely reported. The molecular formula of < 111 > -orientated perovskite $(CH_3NH_3)_3Bi_2Br_9$, $[NH_2(CH_3)_2]_3Sb_2Cl_9$ and $[NH(CH_3)_3]_3Sb_2Cl_9$ was presented in [46]. It should be noted if number of cation is 1 member in the < 111 > -oriented perovskite consists of layers of isolated metal halide octahedron, and can therefore be considered as a 0D perovskite structure [47].

Not only organic nature of *A* cations in the general formula ABX_3 provide the layered structure of the system. The interesting example, potassium and sodium titanates.

The papers [49,50] describe potassium polytitanate **(PPT)** with a layered structure (Fig. 6) formed by a titanium–oxygen octahedral and potassium or hydronium ions in the interlayer space.

The unique structural and chemical characteristics of the organic–inorganic perovskites provide for high interesting and potentially useful physical properties.

Within organic-inorganic perovskite structure structures several possible energy-level schemes can arise (Fig. 7).

In the first case (Fig. 7a) the conduction band of the inorganic layers is substantially below that of the organic layers, and the valence band of the inorganic layers is similarly above that of the organic layers. Therefore, the inorganic sheets act as quantum wells for both electrons and holes. Many of the layered hybrid perovskites are similar to multilayer quantum well structures, with semiconducting, or even metallic, inorganic sheets alternating with organic layers having a relatively large HOMO–LUMO energy gap [2].

In different case metal halide sheets having a larger bandgap are integrated with more complex, conjugated (i.e., smaller HOMO–LUMO energy gap) organic cations, and the well and barrier layers can be reversed (Fig. 7b) [2].

When shifting the electron affinity of the organic layers relative to

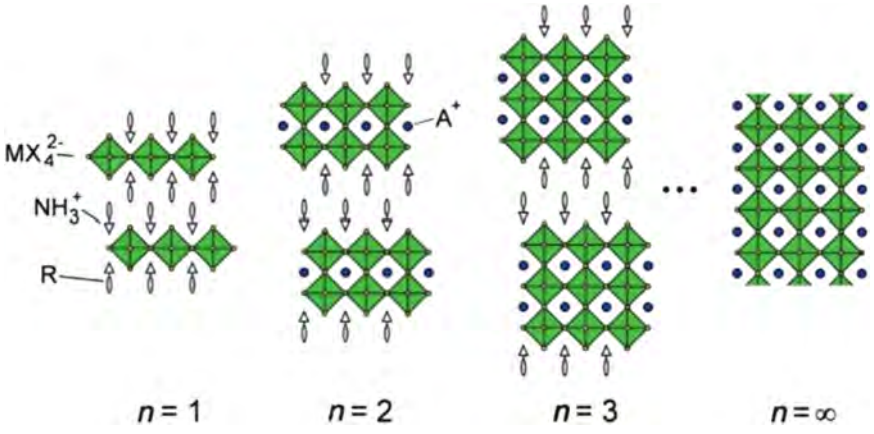

Fig. 3. The < 100 > -oriented hybrid perovskite series with general formula of $(RNH_3)_2A_{n1}M_nX_{3n+1}$. The thicknesses of inorganic slabs increase and toward 3D structure with increasing *n* [45].

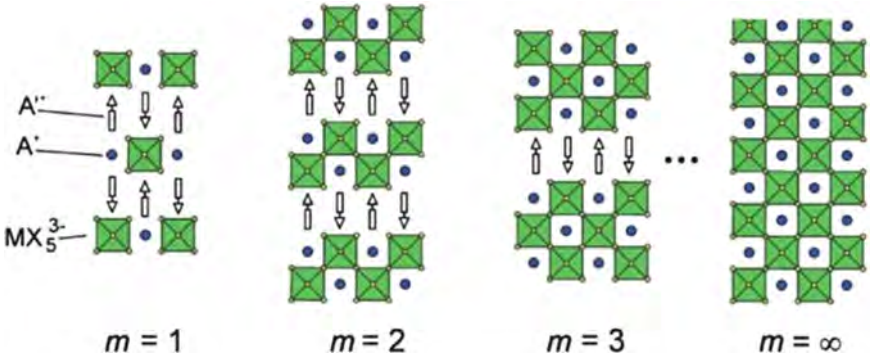

Fig. 4. Schematic representation of the < 110 > -oriented family of layered hybrid perovskites [45].

the inorganic layers, a staggering of the energy levels leads to a type II quantum well structure (Fig. 7c) [2].

3.1.1. Modern topic of 2D perovskite for solar cells

Hybrid lead halide based perovskites that are emerging as one of the most promising light absorbers was initially studied in form of 2D and 3D structures, but 3D perovskites structures were significantly leaders in efficiency. However, the moisture sensitivity of the lead perovskite has not yet been described. It should be noted, that the two-dimensional (2D) perovskites readily formed high-quality films that appeared more resistant to humidity than the 3D analogues. It is therefore of great importance to study and develop alternative classes of moisture resistant perovskite compounds for photovoltaic applications.

As has been described in earlier papers by David Mitzi and coworkers [1–5] 2D perovskites can be structurally derived from the 3D analogue by slicing along specific crystallographic directions and inorganic layers of layered perovskites and comprises 1, 2, 3 or more of metal-halide octahedrons sheets.

2D materials with single metal-halide octahedrons sheets (n=1, n=number of metal-halide sheets in each inorganic layer) do not have electronic properties typically associated with good solar-cell absorbers [51].

Recently, some amount of pioneering papers about 2D layered hybrid compounds based on metal-halide perovskite for increasing a humidity resistant of solar cells have been made [51–53].

Effects of number of metal-halide octahedrons sheets in each inorganic slab (n) on the photovoltaic performances of planar perovskite solar cells was described by Gan et al. [51] and presented in Table 1.

Saparov et al. reported about layered perovskite $(PEA)_2(CH_3NH_3)_2Pb_3I_{10}$for solar cell application (where PEA – phenylethylammonium), demonstrates an open-circuit voltage of 1.18 V and a power conversion efficiency of 4.73% [52]. More importantly, it is relatively stable of presented cells in air containing 52% relative humidity for up to 46 days.

A suitable as moisture resistant absorbers for solar cells based on

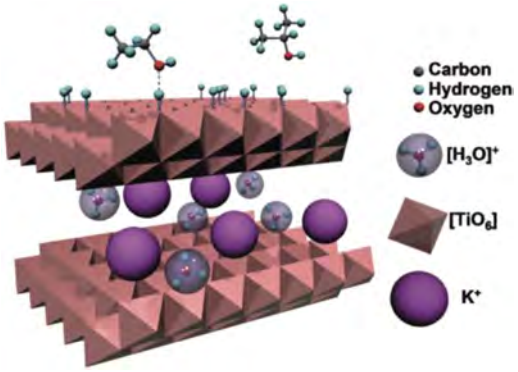

Fig. 6. The layered structure of PPT [49].

2D perovskites system $(n\text{-}C_4H_9NH_3)_2(CH_3NH_3)_{n-1}Pb_nI_{3n+1}$, ($n$=1–4) was presented [53]. From n=3 compound a power conversion efficiency was 4.02%.

In work [54] presented 2D perovskites $(PEA)_2(MA)_{m-1}Pb_mI_{3m+1}$ (PEA – phenylethylammonium, MA – methylammonium, m = 1,2,3) for application as light absorbers in solarcells which show a high stability under humid air. The dependence of m value on the cell performance was reported (Fig. 8) and an efficiency of 3.72% is obtained for $(PEA)_2(MA)_2Pb_3I_{10}$ perovskite cells was shown.

Moreover, lead-free 2D perovskite $Cs_3Sb_2I_9$ [52] and $(CH_3NH_3)_2CuCl_xBr_{4-x}$ [54] are synthesized and studying the optoelectronic properties to explore their potential as light absorber in solar cells.

Although no high device performance has been obtained yet, lots of created 2D layered hybrids lead to versatile approaches for the applications of novel perovskite films with adjustable optoelectronic properties and enhanced stability [53–58].

3.2. 3-D perovskites

Any materials having a crystalline structure like natural $CaTiO_3$ are

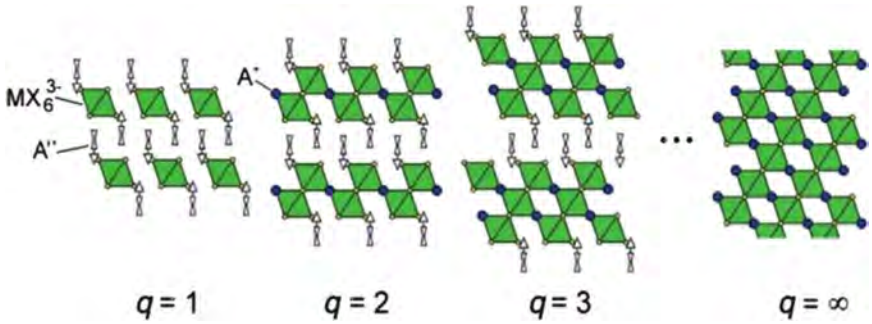

Fig. 5. Schematic representation of the < 111 > -oriented family of layered hybrid perovskites [45].

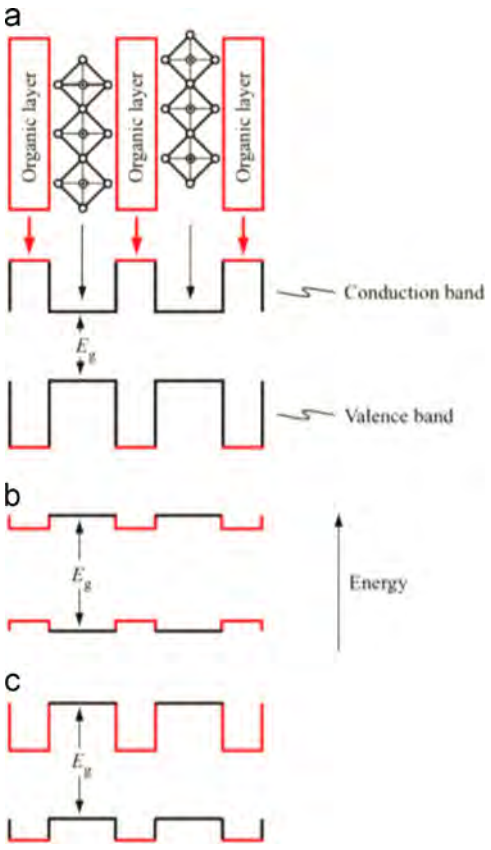

Fig. 7. Schematic organic–inorganic perovskite structure. (a) – A relatively large HOMO–LUMO energy gap and a type I quantum well structure; (b) – a smaller HOMO–LUMO gap result in the well/barrier roles of the organic and inorganic layers being switched; (c) – the bandgaps for the organic and inorganic layers are offset, what leads to a type II quantum well structure [2].

Table 1
Photovoltaic performances of planar perovskite solar cells [51].

Device	Voc (mV)	Jsc (mA cm^{-2})	ff	η (%)
m=1	708	0.48	0.44	0.15
m=2	770	2.38	0.65	1.19
m=3	755	4.48	0.48	1.62

called perovskites. By now there are several hundreds of such materials with diverse properties – ferromagnetic, piezoelectric, thermo-electric, semi-conducting, conductive and superconductive [43,59,60]. As it has been already noted above, Mitzi with the co-authors were the first who paid attention to perovskites and carried out the detailed studies of the optoelectronic properties of such materials. The general formula of nano-hybrid perovskites containing the organic and inorganic parts has the form ABX_3 where A is the aliphatic ammonium, B is the bivalent cation of metals (Pb^{2+}, Sn^{2+}, Ni^{2+}, Pb^{2+}, Mn^{2+} and others) and X is the one-valent anions of halogens I^-, Br^-, Cl^- [59]. More frequently the A component in perovskite is $CH_3NH_3^+$, $NH_2CHNH_2^+$, B–Pb^{2+}, Sn^{2+}. The A and B cations coordinate with 12 and 6 atoms of X forming the cuboctahedral and octahedral structure, respectively. The crystallographic structure and its stability are estimated by the Goldschmidt tolerance factor "t" [61].

$$t = (r_A + r_X)/[2^{1/2}(r_B + r_X)],$$

where r_A, r_B, r_X are the effective ionic radii of the corresponding ions. It is considered that perofskite is stable when t is within the range 0.76 and 1.13 [62]. However, besides the tolerance factor the perovskite stability is defined by a octahedral factor μ, i.e. the ratio of the ionic

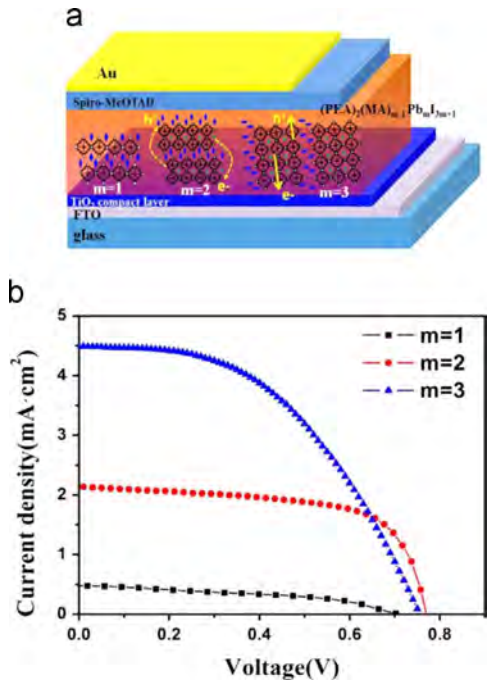

Fig. 8. Planar perovskite solar cell based on $(PEA)_2(MA)_{m-1}Pb_mI_{3m+1}$with different m value construction and performance (a) schematic device architecture, (b) J–V curves [51].

radii r_B and r_X. The value of μ should be within the range 0.442 and 0.895. The A cations and their sizes are: $CH_3NH_3^+$ ~ 0.18 nm, $CH_3CH_2NH_3^{+3}$ ~ 0.23 nm, formamidine – $NH_2CH{=}NH_2^+$ – 0.19–0.22 nm, the B cations are: lead – 0.119 nm, tin – 0.110 nm and the X anions are halogens: iodine – 0.220 nm, bromine – 0.196 nm, chlorine – 0.181 nm. The crystalline structure and the values of the parameters t and μ for more frequently used perovskites $CH_3NH_3PbI_3$, $CH_3NH_3PbI_{3-x}Cl_x$ и $CH_3NH_3PbI_{3-x}Br_x$ are presented in Fig. 9.

The high coefficient of absorption (for $CH_3NH_3PbI_3$ – $1.5{\cdot}10^4$ cm^{-1} at 550 nm), the wide range of absorption (from 350 to 800 nm and higher) and the conductivity over 10-3 S cm^{-3} predetermined a main goal of perovskites as the best absorbers of solar radiation [63].

The binding energy of the electron-hole pair (exciton) in the process of optical excitation is 20–45 meV for $CH_3NH_3PbI_3$ [51,64,65], 55 ± 20 meV for $CH_3NH_3PbI_{3-x}Cl_x$. The charge mobility in perovskites depends on the conditions of their formation and has the value 33 cm^2/V s and 11.6 cm^2/V s for the highly qualitative films of mixed perovskite which were produced by vacuum deposition and through solution, respectively; for perovskite iodide produced through solution this value is significantly less ~ 8 cm^2/V s [38,66]. The dielectric constant is sufficiently high 4.8 and 6.5 for perovskite iodide and bromide, respectively. That means that perovskites can accumulate charges as high-capacitance condensers [67]. All these values are evidence of the fact that optical excitation in perovskites is produced by Wannier–Mott excitons [68], which means in turn generation of free carriers of charges responsible for the photovoltaic effect. The presence of a polar molecule in the center of perovskite promotes polarization and variation of orientation in the electric field. The role of these ferroelectric domains is exceptional for the photovoltaic properties to be manifested [69]. A variation of the dipole moment and cation size of the molecular dipole can have essential influence on the ferroelectric behavior and dielectric constant, as well as on the forbidden zone width.

Depending on temperature, for the polycrystalline films of perovskite iodide and mixed perovskite the authors found two exciton transitions at 740 nm and 765 nm sliding from one into another at temperature 170 K and 140 K, respectively [70]. That is a phase

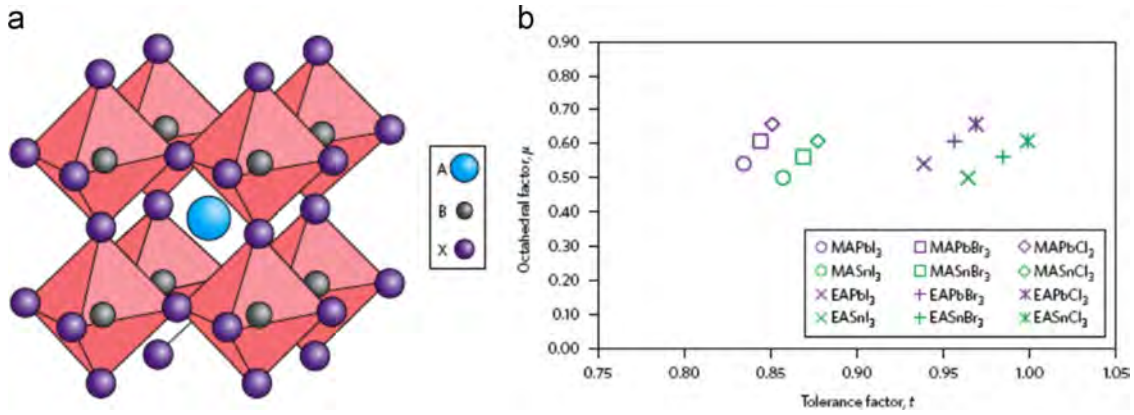

Fig. 9. Perovskite crystal structure and associated tolerance and octahedral factors. a, Cubic perovskite crystal structure. For photovoltaically interesting perovskites, the large cation A is usually the methylammonium ion (CH_3NH_3), the small cation B is Pb and the anion X is a halogen ion (usually I, but both Cl and Br are also of interest). For $CH_3NH_3PbI_3$, the cubic phase forms only at temperatures above 330 K due to a low t factor (0.83). b, Calculated t and μ factors for 12 halide perovskites. The corresponding formamidinium ($NH_2CH{=}NH_2$) based halides are expected to have intermediate values between those of the methylammonium (MA) and ethylammonium (EA; $CH_3CH_2NH_3$) compounds shown Reprinted with permission from ref. [60].

transition in perovskite crystals from a tetragonal structure into an orthorhombic one. A single exciton peak at temperature 4.2 K and 760 nm corresponds to the similar data obtained for perovskite monocrystals. Because of polycrystallinity the two phases are observed at temperature 150 K. It should be noted that in this work an important aspect associated with dimensionality of perovskite crystals produced on different substrates was observed. On a smooth quartz substrate the crystal size was about 500 nm while 60–100 nm on mesoporous Al_2O_3 one. Undoubtedly, for the photovoltaic characteristics the large sizes are advantageous.

The problems of chemical degradation of perovskites and the ways of their stabilization are considered in detail in [71].

In search of the best representative of perovskites a great number of experiments on component variation, i.e. inorganic part and halide, were carried on. For the different halide component the band gap of perovskites is 1.5 eV, 1.55 eV, 2.2 eV for $CH_3NH_3PbI_3$, $CH_3NH_3PbI_{3-x}Cl_x$, $CH_3NH_3PbI_2Br$, respectively, [65]. It should be noted that the size of the organic component can regulate the electronic properties of the inorganic part of perovskite. In [72,73] the length of the organic component (methylammonium, ethylammonium and propylammonium) was varied; the band gaps was estimated as 1.6 eV, 2.2 eV and 2.4 eV, respectively. The conversion efficiency 7.4%, 0.26%, 0.016% was obtained for the mesoporous configuration of cell with a hole-transport material (HTM) spiro-OMeTAD, respectively. A significant decrease in conversion the authors associated with the weak absorption characteristics of perovskites due to weakening an overlapping of the electron orbitals because of increasing the distance between the atoms of lead and iodine. On the contrary, substitution of methylammonium cation with formamidine ($NH_2CHNH_2^+$) leads to increasing the band gap up to 1.43 eV–1.48 eV [74]. With the use of different technologies of perovskite film formation and methods of cell modification the conversion efficiency was obtained from 3.5% to 16.1% [75].

The mixed perovskites are of great interest. Besides the above-mentioned perovskite $CH_3NH_3PbI_{3-x}Cl_x$ considered in detail in the other sections of the survey, attention should be drawn to perofskites like $CH_3NH_3Pb(I_{1-x}Br_x)_3$ and $(NH_2CHNH_2PbI_3)_{1-x}(CH_3NH_3PbBr_3)_x$. Variation of the Br content from 0 to 1 leads to changes in elementary cell parameters, optical absorption, band gap (1.55–2.2 eV) and conversion efficiency from 4% to 12%. The highest value of the conversion efficiency 12.3% corresponds to x=0.2. This cell keeps its efficiency for 20 days even for relative humidity 35% while the conversion efficiency of perovskite iodide for the same period decreases up to 3.5%. The similar compositions have sufficient transparency so they can be easily integrated in buildings under construction (windows, roofs, walls *etc.*) [76]. The same group of the authors studied in detail the conversion data and structural stability of the mixture $(NH_2CHNH_2PbI_3)_{1-x}(CH_3NH_3PbBr_3)_x$. Earlier the attempts to combine perovskites on the basis of methylammonium and formamidine to strengthen adsorption characteristics were made in [74].

In these mixtures the authors found significant changes in electronic structures with variation of content of peroskites on the basis of formamidine and for the mesoporous cells with the use of PTAA as HTM the maximal conversion efficiency 20.3% was obtained. The further studies in this direction should be undoubtedly developed for conversion and operation stability of perofskite cells to be strengthened.

3.3. Solar cell architecture: basic structure

Very shortly in this Part 1, more detailed in Part 2.

The cell efficiency directly depends on design features that define material selection, deposition conditions, compatibility and possibility of purposeful regulation of component interaction. There are two basic kinds of solar cell designs – mesoscopic and planar (Fig. 10). The mesoscopic design is effective for the thin films of perovskites with the maximal degree of mesoporous substrate coverage (metal oxides mainly) or allows complete filtration of oxide with an additional excess layer of perovskite. More simple and technological is the planar cell structure that can be conventional or inverted depending on current direction.

The development of the solar cells on the basis of perovskites started with the mesoporous configuration of cells. Owing to good absorption characteristics of the cells on the basis of dyes, perovskite occupied a place of the dye as nanoparticles (QD) on the surface of mesoporous titanium oxide and afterwards the problem of perovskite solubility was solved by electrolyte replacement with an organic semiconductor – spiro-OMeTAD as a hole-transport material (HTM) [77]. The conversion was achieved 9.7%.

According to the data of photoinduced absorption spectroscopy, titanium oxide participates in the conversion process and so it is considered to be an active component. Variation like mesoporous layer promoted approbation of aluminum oxide [16] as a substrate with high surface. Despite the fact that Al_2O_3 is an insulator the conversion efficiency of this cell increased up to 10.9%. That means that the mixed perovskite ($CH_3NH_3PbI_{3-x}Cl_x$) with such architecture is not only an absorber but also an electron-transport material **(ETM)**. Since aluminum oxide takes no part in the process of charge transport it is called a passive component. The reason for the high conversion efficiency the authors see in higher rate of electron diffusion through perovskite. For

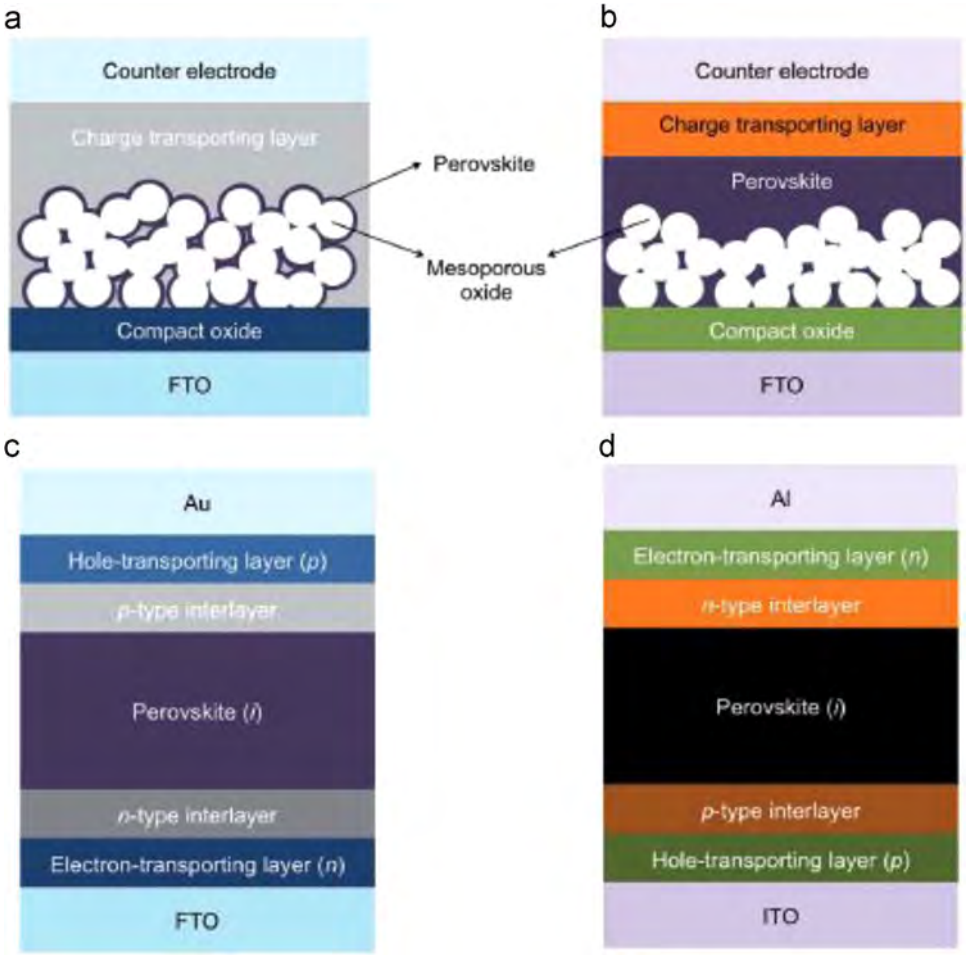

Fig. 10. Schematic diagram of mesoscopic heterojunction solar cells (a) no perovskite overlayer and (b) with perovskite overlayer; and planar heterojunction solar cells with (c) conventional "n–i–p" and (d) inverted "p–i–n" configurations. Reprinted with permission from ref. [77].

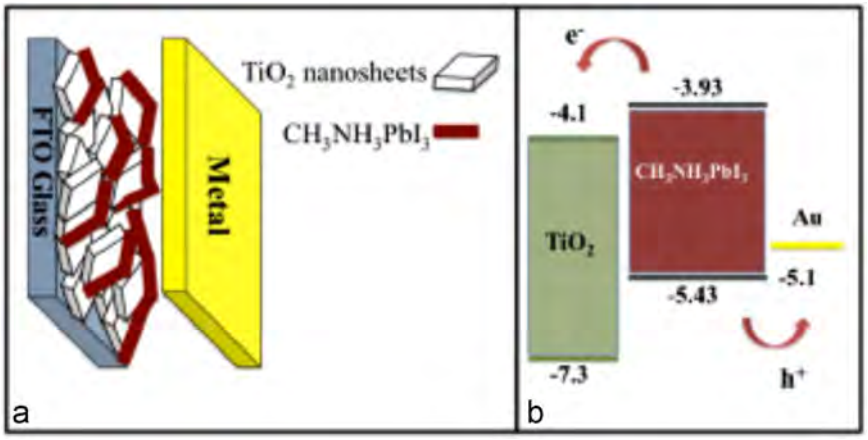

Fig. 11. (A) Scheme of the device structure. (B) Energy level diagram of the $CH_3NH_3PbI_3/TiO_2$ heterojunction solar cell. Reprinted with permission from Ref. [17].

the similar cell configuration, using as a mesoporous substrate the titanium oxide nano-plates oriented in the 001 plane, Etgar with the co-authors obtained the conversion efficiency 7.3% for perovskite iodide without hole-transport component with low intensity of radiation 100 mW/cm^2 (Fig. 11) [17]. These data are evidence that the perovskite nano-crystals can act as hole transporters in solar cells with mesoporous configuration. Further development of such construction is connected with optimization of the fill factor **(FF)** and V_{oc} by way of control of perovskite layer crystallinity.

3.4. Methods of perovskite film deposition

At the same time some papers stated the ideas about creation of determining conditions for deposition of uniform perovskite films taking into account the crystallization features and volatility of organic precursor in the process of spin-coating and thermal treatment. A method of sequential deposition of perovskite precursor solutions (Fig. 12) in the construction with mesoporous TiO_2 proposed by Grätzel [17,20] should be considered to be fundamental. The similar approach, as stated above, was used by Mitzi with the co-authors for

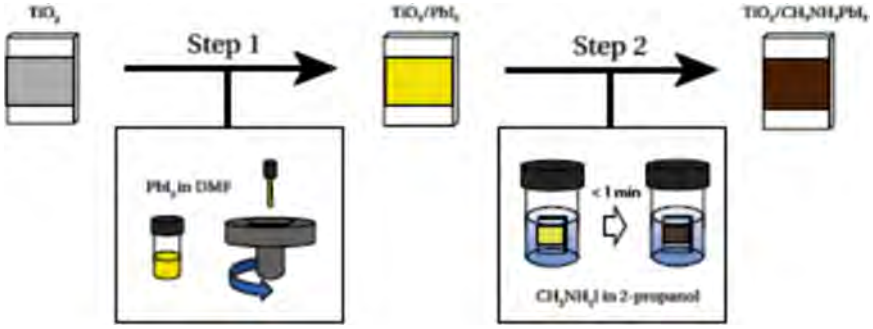

Fig. 12. Scheme that illustrates the deposition of the $CH_3NH_3PbI_3$ perovskite via sequential deposition technique. PbI_2 is first deposited via spin-coating (Step 1) and subsequentialy transformed into $CH_3NH_3PbI_3$ by dipping in solution of CH_3NH_3I (Step 2).

creation of field transistors and light diodes on the basis of perovskites. At first, the PbI_2 solution (the concentration of ~1 M) in dimethylformamide is deposited on mesoporous TiO_2 that is also deposited through the solution of colloidal particles of anatase on a compact titanium oxide layer of 30 nm in thickness. Then the composite film TiO_2/PbI_2 is dipped into the solution CH_3NH_3I in 2-propanol with the concentration 10 mg/ml. This approach allows uniform film formation with the high degree of mesoporous substrate coverage; as a result, for this cell the conversion efficiency of about 15% was achieved with good reproducibility.

In the planar configuration the semiconductor absorber is placed between two transporters of electrons and holes with no mesoporous substrate. As an electron-selective layer one uses dense metal oxides that are also present at the mesoporous configuration of cells as a hole blocking layer to avoid electron-hole pair recombination when the hole-transport component contacts with indium tin oxide **(ITO)** or fluorine-doped tin oxide **(FTO)**. At the initial stage of studies a great difference in the conversion efficiencies of the planar and mesoporous configuration of cells was observed. As an example, the data obtained with mixed perovskites can be presented: 4.9% for the planar configuration and over 9% for the Al_2O_3 mesoporous substrate [18,77]. Nevertheless, the absence of principal restrictions for the effective characteristics of perovskite to be revealed in the planar configuration was justified in subsequent works [22,75] in which the conversion efficiency was achieved within 15–19%.

A vacuum deposition of mixed perovskite precursors (Fig. 13) should be considered as a key point in development of the planar configuration (such deposition was made by Snaith [22]).

Comparison of the conversion values of this method (15.4%) with traditional spin-coating through solution (8.6%) is evidence of how it is important to seek optimal technologies of producing uniform films of perovskite and how it is possible to get the high conversion efficiency with no mesoporous component. In the same aspect, it is interesting to compare two works [78,79] with the use of perovskite iodide and indium tin oxide as a selective electron-transport layer in the form of a compact layer and nano-rod in the mesoporous and planar configurations on glass and flexible substrate, produced by solution-processing and sequential deposition, respectively. In the first case for the mesoporous configuration on glass and flexible substrate the conversion efficiency 8.9% and 2.62%, respectively, was obtained while for the planar one the conversion efficiency was 15.7% and 10.2%, respectively.

Synthesis of perovskite iodide and mixed perovskite by mixing the precursors of methylammonium iodide and lead chloride or iodide of the molar ratio 1:1 in γ- butyrolactone or dimethylformamide is described in detail in [11,17,19]. Then the substrate is heated at the temperature 100 °C for 15 or 45 min for crystallization of $CH_3NH_3PbI_3$ and $CH_3NH_3PbI_{3-x}Cl_x$, respectively. The perovskite films are produced by spinning of a solution in a glove box with the concentration of water molecules and oxygen no more than 0.1 ppm. The above-described method of sequential deposition of perovskite precursors [21,22] includes the stage of film formation from the PbI_2 solution with subsequent dipping into the CH_3NH_3I one. It was noted that on the smooth surface the conversion of perovskite formation even for 45 min is incomplete. This fact confirms the assumption that the diffusion of CH_3NH_3I through the crystalline structure is difficult because the total transformation require several hours. The same process on the mesoporous substrate runs for several seconds. The optimal conditions for spinning time and solution concentration provided the conversion efficiency 12.0 ± 0.5% on average. An additional stage of TiO_2/PbI_2 pre-wetting in 2-propanole for several seconds before dipping into the solution of 2-propanole with CH_3NH_3I gave the conversion efficiency over 15%. The observed effect the authors associated with better filtration of perovskite on TiO_2; an increase in the portion of scattered light (a long-wave response of the cell is improved) and pre-wetting (the CH_3NH_3I concentration decreases) lead to the growth of large crystals of perovskites.

The next step for condition optimization for a qualitative peroskite film to be formed was the work with deposition of vapors of mixed perovskite $CH_3NH_3PbI_{3-x}Cl_x$ under vacuum conditions [22]. Comparison of morphology (Fig. 14) of perovskite films made by solution-processing and vacuum deposition of perovskite precursors revealed advantages of the latter in film uniformity, lack of pores and high degree of substrate coverage with crystallite size up to 400 nm while for the solution-processing methods there is a great difference in the crystallite size 50–400 nm.

A remarkable feature of the method is that it is realized for the planar configuration of cell, the high conversion efficiency 15.4% was achieved with no mesoporous nano-structural layer of metal oxide. Nevertheless, in the subsequent works the stage of vacuum deposition was criticized from the economical point of view. Certainly, attention should be paid to a two-step method comprising deposition by the PbI_2 solution-processing as the first step and the subsequent deposition of vapors of the organic component CH_3NH_3I [24] in the planar configuration of cell as the second one. The studies of the kinetics of precursor reactions along with morphology of formed crystals allowed the optimal conditions for the process with formation of crystals over 500 nm in size, with high degree of dense TiO_2 coverage and surface roughness less 20 nm. The cells produced by that method showed the high values J_{sc}=19.8 mA/cm^2, V_{oc}=0.924 V, FF=66.3% with the conversion efficiency 12.1%. For that moment the latter was the greatest for perovskite iodide in the planar configuration, all the others were less than 10% owing to a small value of the diffusion length of charge carriers (~ 100 nm).

Addressing a problem of the complete conversion in precursor reactions was also reflected in [25] where a three-step method was proposed – solution deposition of precursors PbI_2 and CH_3NH_3I with the ratio 1:1 mol on mesoporous TiO_2, heat treatment at 130 °C until a PbI_2 film is formed and dipping of substrate into the CH_3NH_3I solution at room temperature until perovskite iodide is formed. An advantage of this method unlike sequential deposition (much time for perovskite formation because of difficulties for the

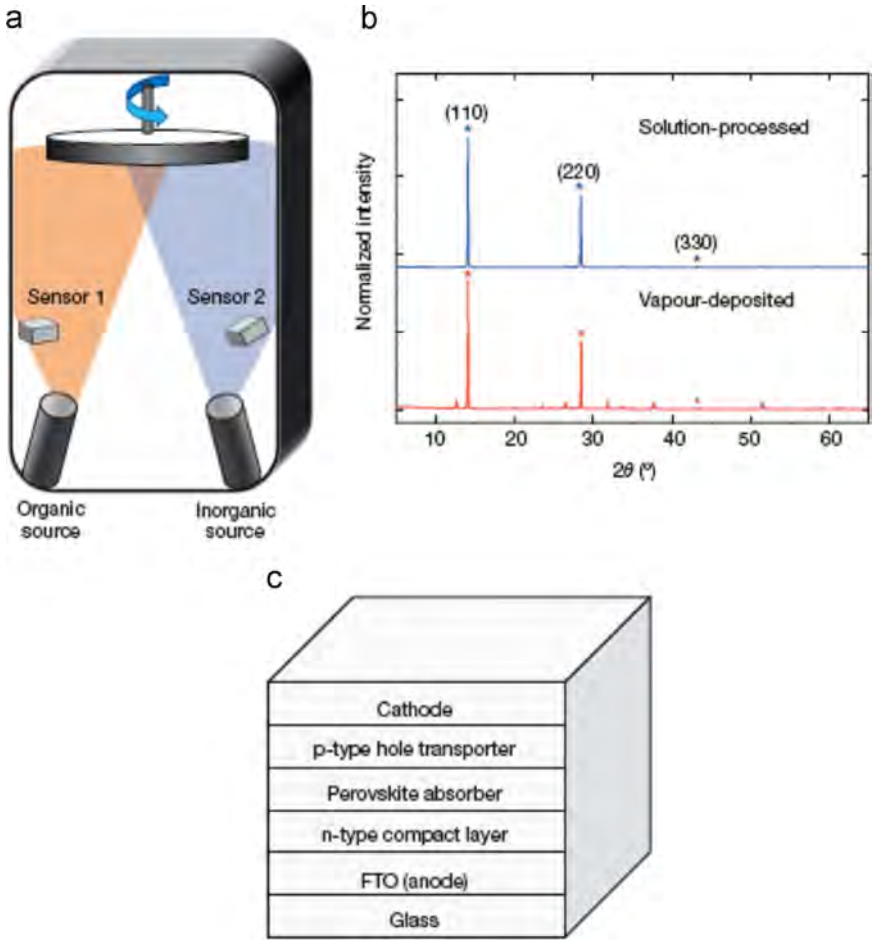

Fig. 13. Material deposition system and characterization. a, Dual-source thermal evaporation system for depositing the perovskite absorbers; the organic source was methylammonium iodide and the inorganic source $PbCl_2$. b, X-ray diffraction spectra of a solution-processed perovskite film (blue) and vapour deposited perovskite film (red). The baseline is offset for ease of comparison and the intensity has been normalized. c, Generic structure of a planar heterojunction p–i–n perovskite solar cell. d, Crystal structure of the perovskite absorber adopting the perovskite ABX3 form, where A is methylammonium, B is Pb and X is I or Cl. Reprinted with permission from Ref. [23].

organic component to penetrate into the layer structure of PbI_2) is pore formation in the process of CH_3NH_3I sublimation, which creates the favorable conditions for complete conversion of perovskite without the presence of unreacted PbI_2. The fact that this method is very perspective is reflected by the electrophysical characteristics of cells on mesoporous TiO_2: the conversion efficiency 10.11%, J_{sc} ~ 18.64 mA/cm^2, V_{oc} ~ 0.868 V, FF ~ 0.625 (for the optimized two-step method for the same configuration of cell the conversion efficiency was 7.23% only).

High reactivity of initial precursors became a base of another technological process of perovskite film formation, namely solid synthesis in the planar configuration of cell.

The main point of the proposed method is to produce independent films of PbI_2 and CH_3NH_3I on corresponding substrates, afterwards their contact, thermal treatment at 135°C and withdrawal of the upper substrate with the help of organic component. The estimation of the structure by the methods of X-ray analysis and optical spectroscopy is evidence of the total conversion of perovskite without residual PbI_2 for 30 min. The maximal conversion efficiencies over 10% and 3.2% were obtained on glass substrate and flexible film, poly(ethylene terephthalate) **(PET)**, respectively.

In general, more developed solution methods [80,81] (spin-coating, blade-coating, inkjet printing and others) are well tested for thin-film technologies of solar cell production on the basis of CdTe, CIGS [82,83]. However, the use of toxic products and high temperature for thermal annealing leads inevitably to an increase in the cost of final products. These disadvantages were fully resolved for the perovskite-based cells of both mesoporous and planar configuration of cells. Almost all the methods were directed to determining the optimal conditions of formation of qualitative perovskite films, i.e. as criterion the morphology of formed films (distribution of crystallites in size, their crystallinity, degree of substrate coverage *etc.*) was thoroughly analyzed. In this direction a more complete picture of morphology development (temperature variation, annealing time, substrate thickness and other parameters) was given by Snaith et al. [22] for the cells on the basis of mixed perovskite with the planar configuration (Fig. 15). A number of the found regularities can be fully used for other configurations of cells.

In the general case, high hygroscopicity of methyammonium leads to degradation of perovskite films before annealing; at the initial stage of solution spinning a sufficient degree of substrate coverage is observed; in the process of thermal treatment because of evaporation and mass transport and from thermodynamic considerations (minimization of surface energy) the pore formation is observed; as a result of annealing (planar architecture) or decrease in the mesoporous substrate thickness (mesoporous architecture) these pores increase in size, which leads to decreasing the degree of substrate coverage with the perovskite film. From these positions the authors propose that in the solution should be an excess of the organic precursors. It was revealed that more optimal temperature of annealing is 90–100 °C and the thickness of perovskite film is 500–600 nm, which ensures high values of the coverage degree and corresponding electrophysical characteristics. The same approach revealed that the minimal thickness of dense TiO_2 with the coverage degree 90% give J_{sc} ~ 17–18 mA/cm^2,

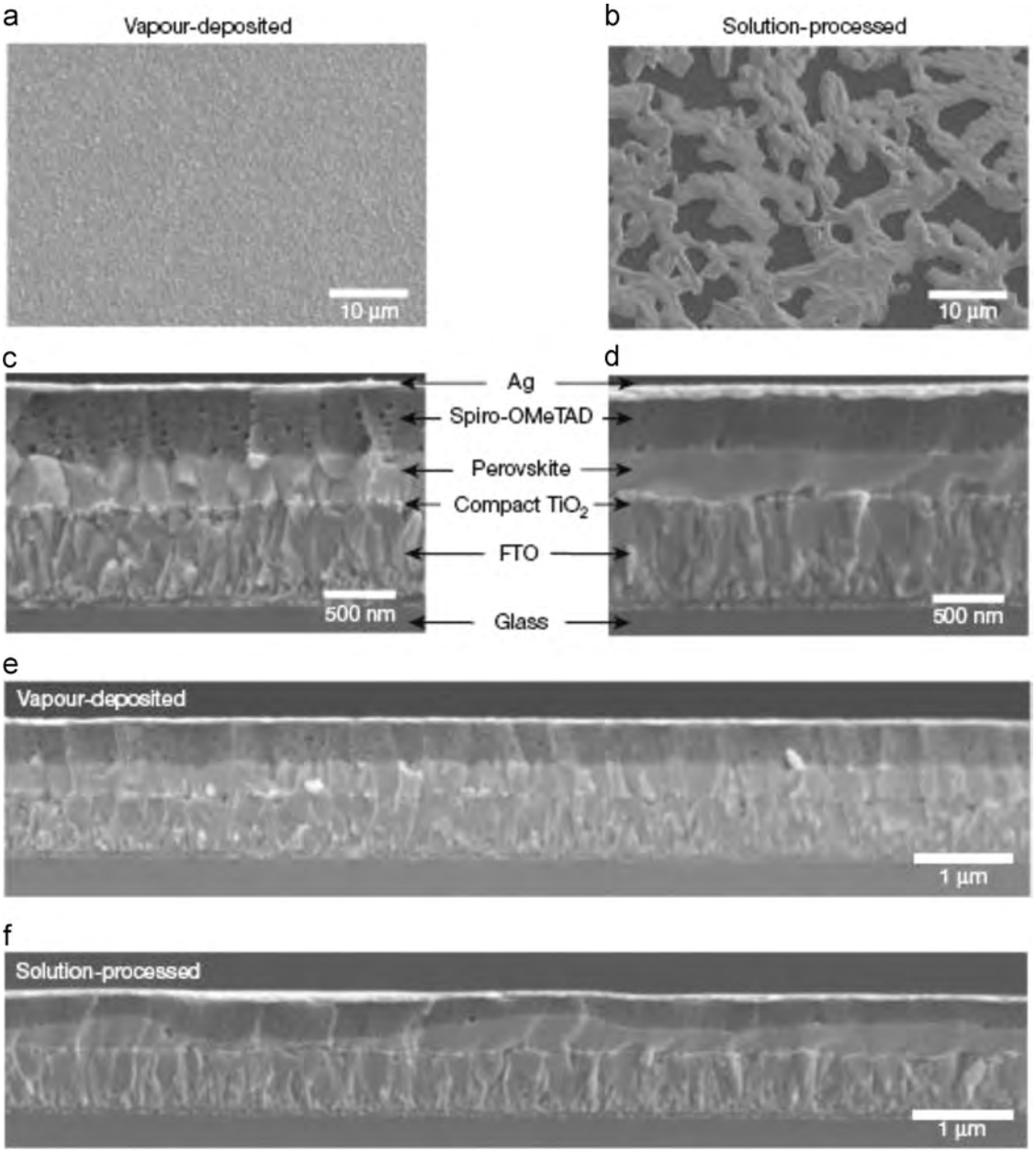

Fig. 14. Thin-film topology characterization. a, b, SEM top views of a vapour-deposited perovskite film (a) and a solution-processed perovskite film (b). c, d, Cross-sectional SEM images under high magnification of complete solar cells constructed from a vapour-deposited perovskite film (c) and a solution-processed perovskite film (d). e, f, Cross-sectional SEM images under lower magnification of completed solar cells constructed from a vapour deposited perovskite film (e) and a solution-processed perovskite film (f). Reprinted with permission from Ref. [22].

V_{oc} ~ 0.8 V, conversion efficiency 8–10%. Cell optimization in degree of perofskite film coverage and thickness of electron transporters (TiO_2 – dense) allowed maximal conversion efficiency 6.7% only. The high degree of coverage ensures maximal absorption of photons and does not allow more unwanted channel of recombination during contact of a hole-transport material of the cell with the surface of selective electrode of electrons (ITO, FTO).

The formation chemistry of mixed perovskite CH_3NH_3I and $PbCl_2$ with variation of their ratio was studied in detail by X-ray photoemission spectroscopy [73]. Owing to the significant difference in the ion radii of Cl^- and I^- while contact of precursors the Cl atoms leave Pb and the excess of electrons in the latter is transmitted to the iodine atoms. As a result of this reaction, the insignificant amount of the chlorine atoms is found on the contact surface of the precursors. More optimal ratio of CH_3NH_3I and $PbCl_2$ was 2.3:1 that ensured the maximal conversion efficiency 6.1%. The authors also revealed that for the excess of $PbCl_2$, as a result of Pb^{2+} cation reduction, metallic lead leading to increasing the conversion efficiency was found.

On the whole, it should be noted that the perovskite film morphology directly depends on crystallization conditions in the process of cell formation. In the conventional cells of both mesoporous configuration and planar one the substrate nature (metal oxide) significantly differs in surface development. Therefore, in the systems under consideration the heterogeneous nucleation of the crystallization process takes place because the energy barrier of the heterogeneous nucleation of the liquid-solid system is much less than that of homogeneous one. The wetting factor is also important; it also decreases the energy barrier of nucleation. As a summary, it should be noted that the crystallization process runs under favorable conditions when the solution deposition of perovskite precursors is realized on a substrate with

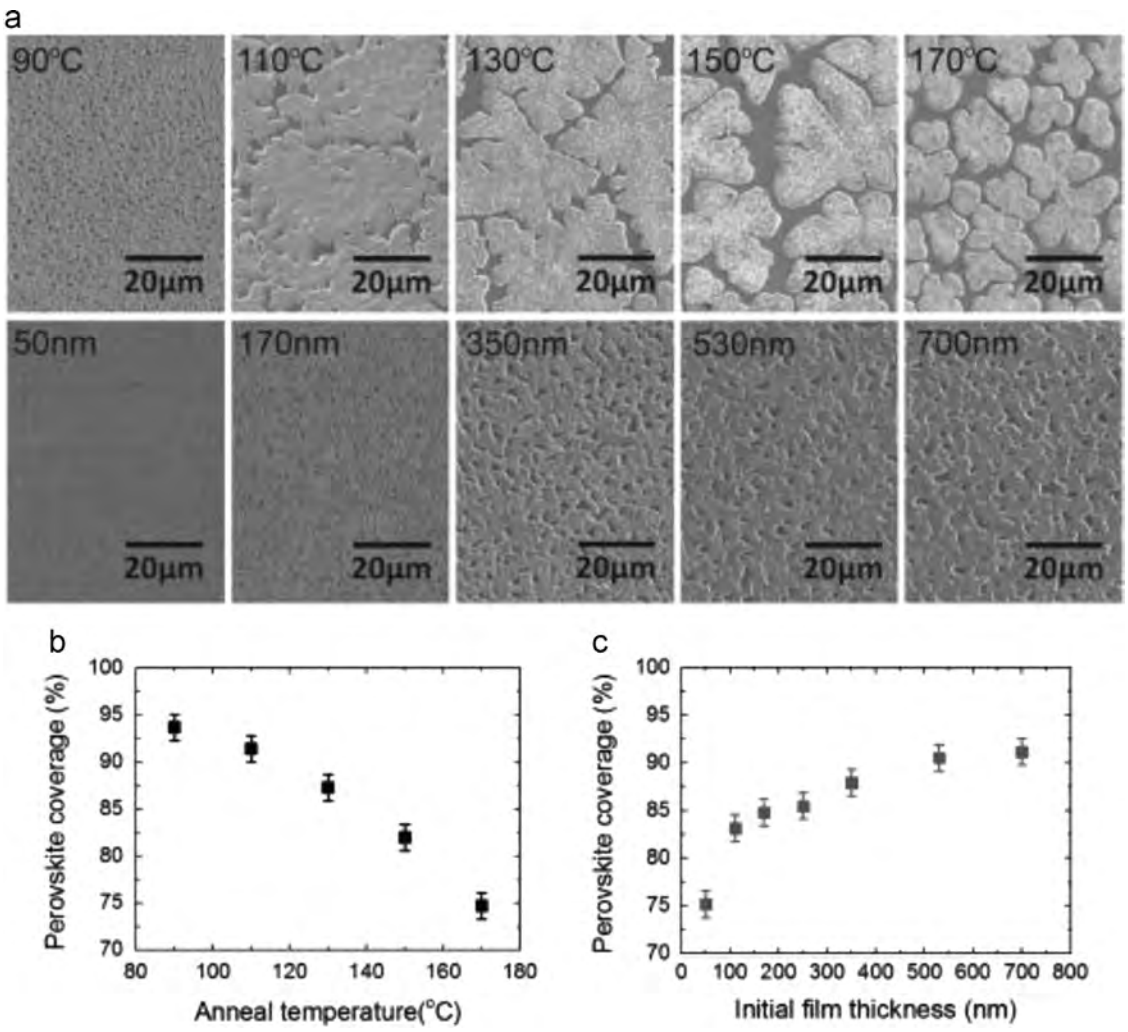

Fig. 15. (a) Top row: SEM images showing dependence of perovskite coverage on annealing temperature, temperature shown on images, holding initial film thickness fixed at 650 ± 50 nm. Bottom row: effect of initial perovskite film thickness, shown on images, with annealing temperature fixed at 95 °C. Perovskite surface coverage as a function of (b) anneal temperature and (c) initial film thickness, calculated from SEM images. Reprinted with permission from Ref. [22].

large surface and high hydrophilicity.

According to the above stated, it is evident that the variation of two important stages of the crystallization process – nucleation and crystal growth by way of optimization of some factors such as solution concentration, precursor ratio, solvent selection, deposition time, solution and substrate temperature – is a key point for formation of a qualitative and uniform film of perovskite without pores and with the high degree of substrate coverage. Additionally, it is necessary to maintain the favorable conditions for high perovskite crystallinity, which ensures the dissociation efficiency of charges, their transport and diffusion length [19,62].

3.4.1. Optimal conditions of OHP crystallization

There are different approaches for regulation and determination of optimal conditions of crystallization; they are solvent selection, regulation of solvent evaporation rate, special additions including chlorine-containing one, annealing by solvent and temperature annealing.

3.4.2. Solvent selection: why DMSO better then DMF

The best solvent in a series of γ-butyrolactone (γ-BL) – dimethylformamide **(DMF)** – dimethylsulfoxide DMSO for formation of qualitative perofskite film is DMSO. However, perovskite produced from this solvent has a number of disadvantages such as incomplete conversion (non-reacted PbI_2) and large polydispersity in crystal size.

These disadvantages can be overcome by mixing the solvents DMSO:γ-BL = 3:7 weight% [28] or DMF:γ-BL = 97:3 weight% [84] and immediate dripping of toluene after the process of spin-coating deposition and perovskite film formation. The formation of stronger complex PbI_2–DMSO as compared to other solvents decelerates the precursor reaction (more favorable kinetic conditions of the reaction) while the process of perovskite crystallization starts with the moment of DMSO molecule evaporation in the process of annealing to which addition of a small amount of toluene makes contribution. The similar approach [85] was proposed for a system with the one-step formation of perovskite from the DMF solution with addition of chlorbenzene to the film under formation. The function of chlorbenzene is to rapidly remove DMF excess, increase precursor solubility, expedite the conditions of supersaturation that leads to nucleation and growth of perovskite crystals. It was noted that toluene dripping does not lead to changes in film color while chlorbenzene addition immediately results in film blackening, which is evidence of perovskite formation. That means that the delay in the crystallization process owing to complex formation is less significant than the variant with rapid nucleation. Argon-cooling of the semi-wet film [86] with subsequent thermal annealing promotes rapid nucleation. Comparison of the cell in the planar device configuration with and without gas-cooling shows that the stage of rapid nucleation (14% and 4.6%, respectively) is more preferable.

Annealing with solvent vapors is of great interest for morphology optimization of perovskite films [87,88]. Particularly, for the annealing

with DMF vapors a rapid growth of the $CH_3NH_3PbI_3$ crystals was observed; this growth is due to diffusion of the solvent molecules (the both precursors are soluble in DMF) and subsequent favorable reorganization of the precursor molecules. Thermal annealing is directed to complete evaporation of solvent and creation the necessary conditions for nucleation and growth of crystals. It is interesting to note that a combination of conventional annealing and rapid one at high temperature ("flash annealing") leads to good results [89,90]. This approach is similar to creation of a supersaturated state in which the stage of the nucleation process of perovskite crystallization accelerates.

3.4.3. Organic additives: acetate, chlorine and others

Organic additives promote the process of perovskite crystallization in the optimal mode [89,90]. The additives should have higher temperature of boiling as compared to the used solvent for precursors and preferable interaction with precursors. Such criteria have diiodoctanes **(DIO)** that have high boiling temperature (332 °C) as compared to dimethylformamide (153 °C). The high jelling capability of DIO with $PbCl_2$ (intermediate compound) allows effective regulation of the rate of perovskite crystallization promoting formation of a smooth film with sufficiently complete coverage of the substrate. This approach was developed in the direction of varying the alkyl chain length and the end group type. For the cells with performance ITO/PEDOT:PSS/$CH_3NH_3PbI_{3-x}Cl_x$/$PC_{61}BM$/bisC_{60}/Ag with the end-group additives I, Cl, Br, the iodine-containing chains 1.4 DIB (the concentration 1 mol%) manifest themselves in the best way. The power conversion efficiency **(PCE)** with this additive was 13.09% while for the cell without it 9.79% only. It is interesting to note that the role of additives is not only optimization of the perovskite crystallization process but also perovskite formation, namely, as a result of thermal treatment, the broken additive links C–X (X is the halogen) become a peculiar source of free halogen for the complete conversion of perovskite formation.

Important diffusion length of exciton in mixed perovskite $CH_3NH_3PbI_{3-x}Cl_x$, good optical characteristics, producible uniform films and realization of these data for the planar cell can be mainly connected with the presence of chlorine ions. It was noted that, as a result of thermal treatment, chlorine is removed as a gas CH_3NH_3Cl (higher volatility than that of CH_3NH_3I), i.e. reacting with the excess of cations $CH_3NH_3^+$. The formed perovskite contains insignificant amount of chlorine; X-ray structure analysis is evidence of the identity of the perovskite iodide spectra with those of perovskite doped with chlorine [73], as well as for special doping of $PbCl_2$ and CH_3NH_3Cl [91]. As a chlorine-containing dopant, NH_4Cl provides the best results of PCE (9.9%) as compared to CH_3NH_3Cl (8.1%) and without additive (0.1%) in the perovskite iodide cell with fullerene as ETM and PEDOT:PSS as HTM. This effect is associated with formation of an intermediate chloride-iodide phase that has the crystalline nature and clearly manifests itself in a X-ray data at the initial stage of thermal treatment. The chloride-enriched phase promotes self-organization of precursors in the process of perovskite formation with formation of a smooth uniform film without pores while other phases (iodide-enriched one) give a great number of unwanted pores owing to sublimation and degradation [92].

The positive effect of the Cl ion presence in perovskite film formation was not established unambiguously. Probably, this phenomenon is similar to those considered above, namely simultaneous action to slow down the crystallization process owing to formation of intermediate compounds and accelerate the nucleation owing to an increase in the rate of solvent evaporation. The large value of the diffusion length of excitons in $CH_3NH_3PbI_{3-x}Cl_x$, to opinion of Du [93], is associated with a significant increase in energy of interstitial defect formation due to decreasing the lattice constants (axis C) owing to a small size of the Cl atom as compared to iodine. Calculating the electronic structure of mixed perovskite, Mosconi [94] found that the Cl atoms at the boundary of perovskite/titanium oxide promote strong electronic overlapping thereby facilitating electron injection from absorber to titanium oxide.

4. Theoretical aspects and photophysics of OHP

4.1. Actual problems of theoretical studies in the field of solar cells based on organic-inorganic perovskites

Uniquely rapid progress observed in recent time in the field of solar cells based on organic-inorganic perovskites is mostly due to an inseparable link of simultaneously implemented theoretical and experimental studies [33,95–97]. On complete ground one can consider that a phenomenon of this cooperation affected successes of technologies, fundamental knowledge of structural, electronic, optical, magnetic, degradation properties of materials and principal features of ready devices.

In general, all the problems where theoretical studies played the fundamental role can be divided into the following sections:

1. electronic structure of ionic and heteroatomic lattice [96,98–100];
2. electronics of zone structure of perovskites [88,97,100,101];
3. defect states in perovskites [96,97,102,103];
4. electronic characteristics of pure and mixed perovskites [33,95–97,104–124];
5. spontaneous electric polarization of perovskites [62,96,125–130];
6. degradation effects in perovskites [110,131–133]
7. hysteresis in volt-ampere characteristics of devices [31,33,95,134].

Let us briefly analyze the most important data of these sections.

4.2. Electronic structure of ionic and heteroatomic lattice

Since the time of Madelung and Ewald it has been known that the binding energy in the ionic and heterogeneous lattice is due to Coulombic forces. That is completely valid for organic-inorganic perovskites for which the calculations of Coulombic energy of Madelung were performed. A great number of the studies of computer simulation of potential energy of ion in different perovskite structures were carried on. The results showed (see Table 2) that the Madelung energy for different ions in perovskite lattices greatly differs from each other and has a high value pointing to significant binding energy of the lattice ions that strongly depends on ion charge.

The latter circumstance proves to be principally important for realization of the photodecomposition processes defining degradation stability in perovskites (see below).

4.3. Electronics of zone structure of perovskites

The second point of the crystal physics after lattice binding energy is a zone structure of crystal. This is due to the fact that in all the problems of solid the crystal chemistry and zone approach play an additional role for each other. Therefore, it is not surprising that great efforts were made to calculate the electronic zones of different perovskites (particularly $(CH_3 - NH_3)PbJ_3$). The calculations were mostly made on the basis of a DFT method and its different variants (including relativistic modifications). A great deal of information concerning this topic is presented in up-to-day surveys [87]. A

Table 2
Electrostatic lattice energy and the Madelung potentials for are range of ABX_3 perovskite structures (cubic lattice, a=0.6 nm) assuming the formal oxidation state of each species. The hybrid halide perovskites are of type I–II–$VIII_3$. Calculations are performed using the code GULP (reprinted from [Frost Butler Brivio Hendon]).

Stoichiometry	$E_{lattice}$ (eV/cell)	V_A(V)	V_B(V)	V_X(V)
I–V–VI_3	−140.48	−8.04	– Welles 59	16.66
II–IV–VI_3	−118.82	−12.93	−29.71	15.49
III–III–VI_3	−106.92	−17.81	−24.82	14.33
I–II–VII_3	−29.71	−6.46	−14.85	7.75

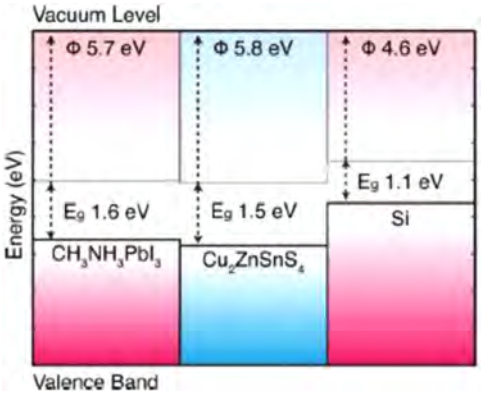

Fig. 16. Valence band ionization potentials of $MAPbI_3$ with respect to the vacuum level. Calculations were performed on the non-polar (110) surface with stab thickness of 25 A and a vacuum thickness 15 A. The Kohn-Sham eigenvalues (PBEsol) are corrected by the bulk quasi-particle energies (ΔE = 0.2 eV) (reprinted from [61]).

principal moment in this problem is that the electronic structure prove to be direct but dependent on collective position of cations $CH_3 - NH_3^+$; although an electronic spectrum (particularly, the width of the forbidden zone) strongly depended on a composition of ABX_3 perovskite. As applied to a base material $(CH_3 - NH_3)PbJ_3$, the electronic structure is so as presented in Fig. 16.

It is important to note that the values of effective masses for holes and electrons (in the approximation of parabolic zones) were $0.12m_0$ for holes and $0.15m_0$ for electrons. Unusual was the study result of how the forbidden zone width depends on elementary cell size. Indeed, the deformation potential calculated for the forbidden zone

$$\alpha_v = \frac{\partial E_g}{\partial \ln V}$$

proved to be positive (α_V^R = 2,45 eV) for $(CH_3 - NH_3)PbJ_3$. This is radically different from the behavior of majority of semiconductors (R is a point at the border of the Brillouin zone). With the above given formula it is possible to discuss how the forbidden zone width depends on ion size for ABX_3 perovskites. The quantum calculations confirm such a simple analysis.

4.4. Defect states in perovskites

Great experience in semiconductor material science shows that an overwhelming majority of the electronic properties of semiconductors can be explained and predicted by studying an electronic spectrum influenced by defects induced in the electronic structure of ideal crystal. In this connection, great interest of the theorists from different groups in this problem is understandable (Wan-Jian Yin et al., Du et al., De Angelis's et al. and others) [87,93,94]. They studied in detail by diverse variants of DFT how the electronic spectrum of perovskite changes after introducing different defects in crystal. From the view point of the electronic properties, most significant are the results of Wan-Jian Yin and co-authors who found an unusual physics of defects in $(CH_3 - NH_3)PbJ_3$ (see Fig. 17) [88].

It was revealed that all the 12 kinds of defects cause both shallow (donor and acceptor) levels and deep ones. It is more essential that in $(CH_3 - NH_3)PbJ_3$ a dominating donor and a dominating acceptor are MA_i and V_{pb}. The both defects have low and comparable energy of defect formation (here MA_i means a methylammonium cation in the internodal position). From the physical point of view, the low energy of MA_i defect formation is associated with weak Van der Waals interaction while the low energy of Pb vacancy formation is due to an antibonding state of the S and P orbitals between the atoms of Pb and I. Since these states (donor and acceptor) are extremely close to the borders of the zones (and even for some cases they prove to be in the permitted ones) then these defects have no influence on lifetime of carriers. In contrast to this, there are deep levels of defects potentially being the killer centers for carriers but they have much higher energy of defect formation.

The fact that internodal iodine, in opinion of Du with the coauthors, causes a deep recombination center for some low-energy configurations is under dispute. Attention was paid to a level (1+ /3+) associated with a lead atom state at the position of iodine since the indicated alternations of the charge states are characteristic of U-negative defects potentially capable of electronic stimulations of atomic reconfigurations.

In recent time the electronic states associated with such defects as boundaries (particularly, twins) are actively studied. There are quantum-chemical ides that they can cause deep recombination centers (see [97]). These conclusions require thorough coordination with experiments owing to great arbitrariness of selecting an atomic structure for boundaries.

4.5. Electronic characteristics of pure and mixed perovskites

The studies of the comparative properties of mobility and lifetime of electrons and holes for crystals $(CH_3 - NH_3)PbJ_3$ and $(CH_3 - NH_3)PbJ_{3-x}Cl_x$ became a reason for very great disputes. A real paradox was found: a chlorine addition to perovskite $(CH_3–NH_3)PbJ_3$ inevitably leads to a disorder in the lattice and hence to worsening the electronic characteristics of the material but an opposite fact was found – an increase in mobility of charge carriers and their lifetime more than an order. One of the interpretations is that chlorine does not create the nodal states but plays a role for technologies of maling better cells. However, there are a number of the studies of radiographic analysis where it is indicated that chlorine can substitute some atoms of iodine. Note that the last variant is in agreement with general thermodynamic concepts about substitution alloys because it is hard to imagine the circumstances of how the electron-similar ions while mixing do not reduce free energy of crystals. Somehow or other, it is interesting to discuss the circumstances whether the real physics of solid allows understanding why chlorine substitution of some iodine atoms improves the electronic properties of perovskite. One approach is connected with ideas that a decrease in a size of the elementary cell when the chlorine atom is introduced leads to an increase in energy of defect state formation like internodal iodide that, as assumed, is an active center for free carriers. Another variant of explanation is based on the assumption that the great number of chlorine atoms located at iodine positions makes the collective motion of methylammonium cations difficult thereby weakening the electron–fanon interaction (ideas of Even et al. [111–115]). However, a less exotic mechanism of improving the electronic properties can be assumed. Indeed, the substituting ion of Cl_s and the internodal atom of iodine have, from the view point of the elasticity theory, sign-opposite dilatations and so they are attracted. While coupling, such defects neutralize their dilatation charges and increase the mobility of electrons and holes. Moreover, approaching to nodal chlorine, the internodal atom of iodine changes its potential (particularly, its central part), which has the immediate effect on the capture cross section for carrier recombination. That inevitably increases the lifetime of recombining electrons and holes. Thus, one can equally explain (for high and low concentration of Cl_s) a simultaneous increase in mobility and a decrease in intensity of the recombination processes. Note that other mechanisms have no such explanation.

Another very important moment is the special features of recombination dynamics (see Fig. 18); they have recently found by Dyakonov et al. [117].

It is seen that after switching off the light pulse there is a decrease in the carrier concentration with time; kinetics of this decrease has a number of the special properties. First, the characteristic rate of decreasing depends on initial intensity of the light pulse; the relaxation rate decreases with reducing the intensity (left figure).

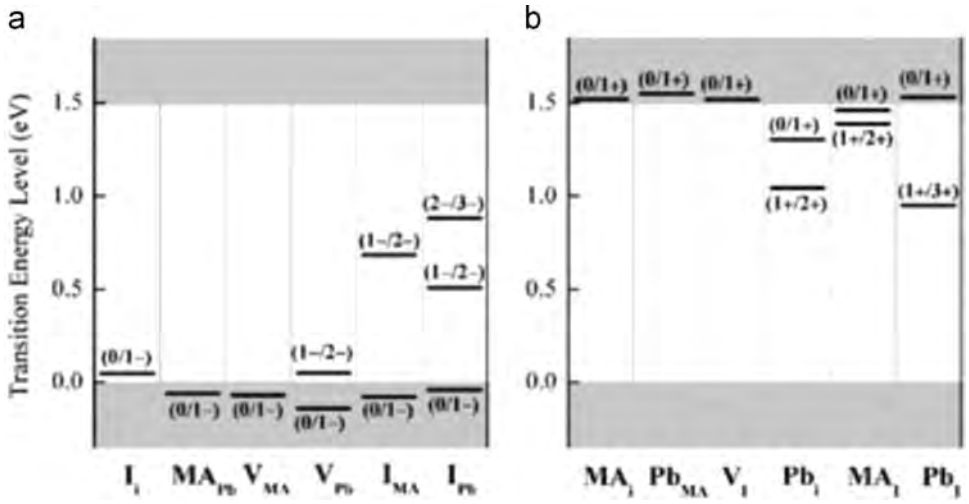

Fig. 17. The transition energy levels of (a) intrinsic acceptors and (b) intrinsic donors in $CH_3NH_3PbI_3$. Zero in energy is referred to the VBM (reprinted from [88]).

Further, an order of the recombination reaction increases from 2 (at 1 "sun") to 2.26 (at 0.1 "sun") and to 2.72 (at 0.01 "sun"). At the same time, if the kinetics of recombination is written as

$$dn/dt = -k_r(np - n_0p_0),$$

where n and p are the concentration of electronic holes and k_r is the recombination coefficient then it is seen from the figure that k_r increases with the raise in intensity (right figure) but the absolute dependence k_r on this intensity become weaker (i.e. $dk_r/dI < 0$). How is that combined? Dyakonov et al. [117] noted a very non-trivial physical picture allowing realizing so unusual experimental dependencies. In our work [120] an attempt was made to construct possible models of this unusual phenomenon.

The first model is based on a hemin recombination idea of Onsager. On the basis of the approach developed by Mozumder, the kinetics of the probability of the pair of carriers to remain non-recombining was described. This kinetics proved to be dependent on diffusion coefficient of electron and hole being in potential interaction with each other. If the polaron effect is taken into account, i.e. the dependence of effective mass of carriers (and mobility as well) on degree of crystal polarization (the latter depends on light pumping) then it is possible to obtain different rate of recombination for different degrees of pumping. That explains the left part in Fig. 18. However, the right figure remains unexplained.

The second model is connected with a ferro-electronic state in perovskite. Indeed, if the Onsager hemin recombination is considered then with taken into account an electric field induced in domain by polarization (a value of this polarization field can be regulated by screening with free carriers from light pumping) it is possible to obtain for the probability of recombination rate of non-recombining carriers a dependence on pumping value. The left part in Fig. 18 can be explained by that fact.

The third model can be constructed by combining a model of three-particle recombination of Thomson [121] and a theory of recombination of Shockley–Read [124]. If one takes into account a level of attachment besides that of recombination (somewhere in the middle of the forbidden zone) then when the pumping decreases the Fermi quasi-level descents and after crossing the second attachment level the second recombination level turns into that of attachment so that the recombination rate decreases, which fully explains the left part in Fig. 18. The right part in Fig. 18 can be obtained if a dependence between the position of the attachment level and recombination one is taken into account then indeed for some parameters (temperature, depth of level formation and pumping) it is possible to obtain the increase of an order of the recombination reaction, i.e. k_r will increase when the pumping decreases ($dk_r/dI < 0$). Thus, the left and right parts in Fig. 18 can be in agreement with each other if two defect levels in the forbidden zone of perovskite, not one, are taken into account.

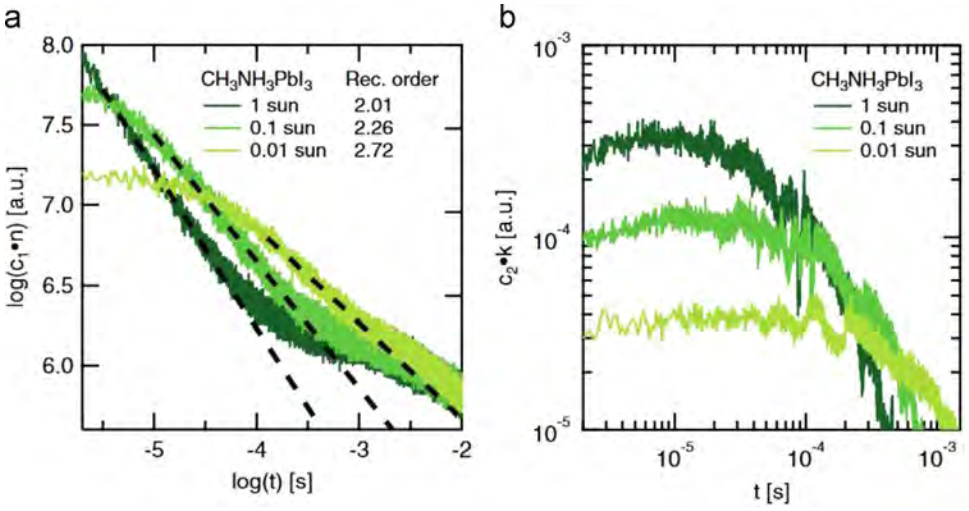

Fig. 18. Recombination dynamics of carriers in perovskite $(CH_3–NH_3)PbJ_3$ under light impulse with different intensity: (a) concentration dependence of carriers; (b) time dependence of recombination coefficient (reprinted from [33]).

Table 3
Calculated properties of four hybrid lead halide perovskites from density functional theory. The molecular dipole (D) is given in Debye, calculated by vacuum B3LYP/6–31 G* in GAUSSIAN. The pseudo-cubic lattice constant ($a = \sqrt[3]{V}$) in A; the lattice electronic polarization (ΔP) in μC/cm^2; and the rotation barrier (E_{rot}), calculated by PBESot in VASP. The nearest-neighbour dipole interaction (E_{dip}) in kJ/mol is estimated from a point dipole calculation (reprinted from [33]).

Cation	*D*	*a*	*ΔP*	E_{rot}	E_{dip}
NH_4	0	6.21	8	0.3	0
CH_3NH_3	2.29	6.29	38	1.3	4.6
CF_3NH_3	6.58	6.35	48	21.4	42
NH_2CHNH_2	0.21	6.34	63	13.9	0.03

4.6. Spontaneous electric polarization of perovskites

The presence of asymmetrical cations CH_3–NH_3^+ in perovskite leads to quite new unique properties of this material. The detailed studies on the basis of DFT allowed calculations of the different parameters of molecular cations. The values of molecular dipoles (in Debyes), the size of pseudocubic lattice (a) in Angstroems, lattice electronic polarization (ΔP) in μC/cm^2, energy of rotation barrier (E_{rot}) and energy of dipole interaction of the nearest neighbors (E_{dip}) in kJ/mol were calculated. These values shown in Table 3 can be compared with the similar crystal parameters (for example, thermal energy). It is seen that many of them for the (CH_3–NH_3)PbJ_3 material have intermediate values. On the basis of all these data it is possible to make conclusion about the presence or absence of the ferro-electric state for specified temperature.

The ferro-electric state existence, in opinion of Frost [33], has a number of far-reaching consequences. First, these authors paid attention to the fact that in a current-carrying state the preferable paths of motion with minimal crossing are formed for electrons and holes. This geometric separation of paths of electron and hole motion decreases the intensity of the recombination processes. It can be noted that an increase in pumping screens a polarizing field of the domains, which increases the recombination intensity. That means that for large "sun" the rate of recombination increases and the regularities of the left part in Fig. 18 manifest themselves. Whether the right part in Fig. 18 can be explained on that basis remains beyond theoretical analysis. Another special feature of the effect of the ferro-electric state on the device properties is that the value of idling voltage can be higher than the width of the forbidden zone. This effect was not also considered theoretically.

4.7. Ultra-long carrier lifetimes and diffusion lengths

While the hybrid (organic-inorganic) organohalide perovskite **(OHP)** solar cells represent the recent breakthrough in photovoltaic applications, the origin of this rapid success is not yet clear from fundamental physics point of view. Despite the abundance of the applied studies on this topic, experimental effort towards understanding the fundamental transport and photophysical properties of these materials is lacking. For instance, a possibility of high charge carrier mobility has been considered as one important factor that contributes to the excellent photovoltaic performance of hybrid lead halide perovskites. Yet, an unambiguous determination of the intrinsic mobility in these materials is missing. Existing experimental values in similar materials range from 0.6 to 50 cm^2 V^{-1} s^{-1}. However, most of the important transport and photophysical parameters, including the above carrier mobilities, lifetimes and recombination rates, were so far measured either in materials different from those relevant for high-performance solar cells (e.g., in metallic tin-halide instead of insulating lead-halide perovskites, or perovskites that adopt 2D layered rather than 3D cubic structure) or under the conditions less relevant to applications (e.g., at ultrashort timescales, instead of steady-state experiments).

Recently reported artifact-corrected Hall effect and steady-state photoconductivity measurements in thin films and single crystals (e.g. of exemplary hybrid perovskites, $CH_3NH_3PbI_3$ and $CH_3NH_3PbBr_3$, of current interest for photovoltaic applications), allowed to independently determine the density of photogenerated carriers, n_{Hall}, and the intrinsic mobility, μ_{Hall}, directly and without assumptions unavoidable in other methods, including ultrafast spectroscopic techniques and space-charge limited current measurements. It is found, in a wide range of illumination intensities that represent most common excitation conditions, the dynamics of photocarriers is governed by a bimolecular *e–h* recombination with a very small recombination coefficient, γ ~ 10^{-11}–10^{-10} cm^3 s^{-1}, which is 5–6 orders of magnitude smaller than the value expected from the Coulomb capture cross section considerations and is comparable to the smallest γ observed in the best direct-band inorganic semiconductors, such as GaAs. In addition, the carrier lifetime, τ, and diffusion length, *l*, estimated in a straightforward way from those measurements, are found to be remarkably long (τ ~ 30 μs and l ~ 23 μm in thin films, and ~ 5.7 ms and ~ 940 μm in single crystals), while the intrinsic Hall mobilities are moderate (μ_{Hall} up to 60 ± 5 cm^2 V^{-1} s^{-1} in single crystals). So this experiments provide the first direct and unambiguous steady-state measurement of a suppressed photocarrier recombination and trapping, leading to extremely long carrier lifetimes and diffusion lengths in hybrid perovskites. While confirming some of the recent theoretical predictions [33], these results open important questions on the physical origins of the intrinsically low carrier mobility, suppressed *e–h* recombination and the miniscule trapping in these materials synthesized via inexpensive vapor or solution based routes at temperatures close to room temperature. Based on observations, it was proposed that these properties might be brought about by a new type of polarons formed by rotational reorganization of the organic methylammonium dipoles around the charge carriers or defects.

Pure $CH_3NH_3PbI_3$ samples are highly resistive in the dark ($\rho \geq 100$ GΩ), and thus one should utilize a steady-state photoexcitation (λ = 465 nm) to generate a population of carriers to be able to measure a photo Hall effect [36]. In $CH_3NH_3PbBr_3$ single crystals, it was possible to measure a dark Hall effect as well, because these crystals are weakly conducting in the dark (at a level of ~ 50 MΩ).

4.7.1. Strongly suppressed electron-hole recombination and new polarons concept

Electron-hole recombination in direct-gap inorganic semiconductors is described by a coefficient γ equal to the product of a recombination cross section, *s*, and thermal velocity, *v*, of charge carriers ($v \approx 10^7$ cm s^{-1} at 300 K): $\gamma = sv$. The cross section *s* for charged species is defined by the Coulomb capture radius (see below), in which case $s \sim 10^{-12}$ cm^2 in typical inorganic semiconductors at room temperature, thus leading to the recombination coefficient, γ ~ 10^{-5} cm^3 s^{-1}. Experimentally, however, most direct-gap inorganic semiconductors exhibit γ ~ 10^{-10} cm^3 s^{-1} in high-purity single crystals [135] In any case, the recombination coefficient γ determined here for solution-grown hybrid perovskites is comparable to some of the best values obtained in pure inorganic semiconductors and is at least 5–6 orders of magnitude lower than the value predicted by the Coulomb capture cross section. In a physically different case of disordered semiconductors with a diffusive charge transport, recombination of charge carriers is often described by the Langevin model with an *e–h* recombination coefficient, $\gamma_L \sim e\mu/\varepsilon_0\varepsilon_r$, where ε_0 and ε_r are the dielectric permittivities of vacuum and the material, respectively. For disordered (polycrystalline) perovskite films with the experimental μ_{Hall}=8 cm^2 V^{-1} s^{-1}, the formally calculated Langevin coefficient is: $\gamma_L \sim 2 \cdot 10^{-6}$ cm^3 s^{-1}, which is about 5 orders of magnitude greater than γ experimentally determined above. This comparison clearly shows that *e–h* recombination in hybrid perovskites cannot be described by the Langevin theory in diffusive transport regime.

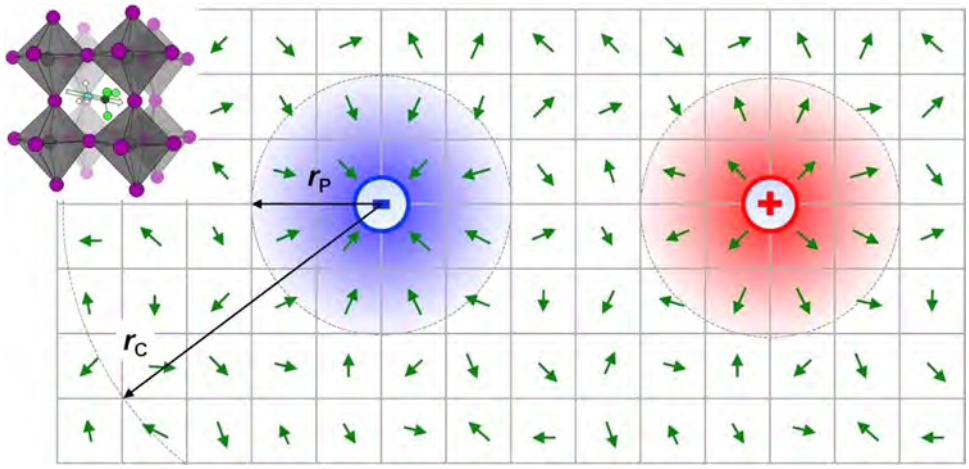

Fig. 19. Schematics of the polaron pair model. Charge carriers, charged impurities or traps can induce a rotational reorganization of the nearby CH_3NH_3 electric dipoles (green arrows) at the length scale r_P away from the charge, leading to formation of a polaronic well and creating an energy gain. The characteristic radius r_P is defined by competition between electrostatic and thermal energies (see the main text). Polaronic wells of oppositely charged polarons can effectively repel each other at a short range, because of a competition between the polarons for aligning the dipoles, thus creating a barrier for recombination. The Coulomb recombination radius, r_C, calculated *without* taking into account any local dipolar screening is greater than r_P ($r_C > r_P$), suggesting that the local rearrangement of dipoles around a charge can efficiently screen it, leading to a reduced Coulomb capture cross section. A similar mechanism may also describe "passivation" of uncharged defects (trap states), thus reducing their trapping cross section. The structure of hybrid perovskite unit cell with a polar methylammonium molecular cation at the center is also shown.

Rather small recombination coefficients γ are also extracted in highly disordered perovskite thin films, in which robust long-range ferroelectric order is unlikely, and CH_3NH_3 dipoles are expected to be orientationally disordered, suggesting that an additional mechanism could be implicated in a strong suppression of *e–h* recombination and trapping in these samples. According to the recent theoretical calculations by Walsh et al. [33], these dipoles carry a significant dipole moment, p = 2.29D, and create a rough local potential landscape, but can be easily rotated or locally aligned by overcoming a small rotational energy barrier, U_{rot} ~ kJ/mol ($1.6 \cdot 10^{-21}$ J or 10 meV per dipole). It has been proposed that a charge carrier moving through the perovskite lattice (or trapped at a defect) induces a local orientation of the surrounding dipoles by aligning them along its electric field, $E = e/(4\pi\varepsilon_0\varepsilon_r \cdot r^2)$, which results in an interesting type of polaron, the ***dipolar polaron***, with the Coulomb field partially screened in the vicinity of the charge (Fig. 19). This leads to an overall energy gain and an increase of the binding energy of the polaron. To estimate the size of the "polarized" region, we note that potential energy of a dipole p in an external Coulomb field E must be sufficient to overcome the rotational energy barrier: $pE \geq U_{rot}$, which for an average $\langle\varepsilon_r\rangle$ ~ 10 gives the radius of the polarized region surrounding the charge, r_P ~ 1 nm (10–20 unit cells, assuming the lattice parameter of 0.629 nm). On the other hand, the Coulomb escape radius calculated without any local dipolar screening effects (that is, defined as the distance between an electron and a hole, at which their Coulomb energy is comparable to the thermal energy, $e^2/(4\pi\varepsilon_0\varepsilon_r r_C) \approx k_B T$) is r_C ~ 5 nm. Even though this is a very crude estimate, it shows that a dipolar polaronic well can be formed around a charge carrier (or a charged impurity/trap) within the length scale of its unscreened Coulomb cross section ($r_P < r_C$), thus allowing the screening to take full effect and minimize the sensitivity of charges to the presence of each other at the length scales, where Coulomb attraction would otherwise lead to unavoidable carrier recombination.

At shorter length scales, the oppositely charged polarons may interact with each other not only directly via their Coulomb field (screened by polarization), but also indirectly via the interaction of their polaronic dresses (that is, via the electric field of their aligned dipoles). The indirect interaction of polaronic wells can be repulsive even in the case of oppositely charged polarons [39], since when the polarons are sufficiently close to each other, closer than depicted in Fig. 19, they compete for aligning the same dipoles, thus partially disturbing the optimal arrangement of each other's polaronic dress and decreasing the polaron binding energy. This effect may lead to an increase of the total energy of the system of two polarons, effectively causing repulsion between them at very short length scales [39], which suggests that polarons gain energetically if they stay away from each other. While comprehensive numerical analysis of such a repulsion in hybrid perovskites is beyond the scope of this work, we note here that, due to both the short-range repulsive barrier between the oppositely charged polarons and screening of the Coulomb attraction at longer length scales, recombination of photocarriers can be strongly suppressed. This mechanism might contribute to the strong suppression of recombination rates in hybrid perovskites. The proposed dipolar polaron can also explain the relatively small intrinsic carrier mobilities that have been experimentally obtained via careful Hall effect measurements.

The most surprising result from the experiments however is that the trapping regime is not observed in these materials down to extremely low carrier densities, n ~ 10^{15} cm^{-3} in thin films and ~ $5{\cdot}10^{12}$ cm^{-3} in single crystals. Indeed, if present, such a regime would manifest itself as a linear $\sigma_{PC}(G)$ dependence. The absence of trapping is exactly the reason why bimolecular *e–h* recombination dominates down to such low carrier densities, leading to remarkably long carrier lifetimes and diffusion lengths. In direct-band inorganic semiconductors, even though similarly small values of γ ~ 10^{-11}–10^{-10} cm^3 s^{-1} are observed in pure crystalline samples, achieving a *ms* carrier lifetime and nearly a *mm*-long diffusion length is unheard of, simply because other recombination mechanisms (for instance, trapping, recombination centers or Auger processes) onset at higher carrier densities and dominate, given the rather small *e–h* recombination coefficient. Indeed, in well optimized direct-band semiconductors, such as GaAs, InP or InAs, τ and l are at best a few μs and a few tens of μm, respectively [39,135]. Therefore, the right question to ask is what mechanism allows the hybrid perovskites to be must less sensitive to defects and traps that must be present in these non-optimized, solution or vapor grown materials at large concentrations. The likely explanation is the same *dipolar polaron* introduced above. Indeed, typical medium-energy traps in semiconductors have energies relative to the band edge, δU_{tr} ~ 0.1–0.3 eV. Furthermore, a suspected deep trap state in $CH_3NH_3PbBr_3$ single crystals might be located at ~ 0.8 eV. Typical size of the traps is of the order of a lattice constant, δr_{tr} ~ 0.5 nm. The same effective "force" that causes a mobile charge

carrier to "fall" in a trap and get localized would also cause an electric dipole in the vicinity of the trap to rotate and assume a certain orientation. In hybrid perovskites, this can occur, since the potential barrier for such rotation, U_{rot} ~ 10 meV, is smaller than the energy gain associated with a dipole-trap interaction: $p\cdot\left(\frac{1}{e}\cdot\frac{\delta U_{tr}}{\delta r_{tr}}\right)$~ 10–75 meV (for p = 2.29D). Therefore, the dipoles can rearrange themselves around a defect and reduce its trapping cross section. Such a "defect decoration" is reminiscent of the recently observed trap healing effect at two-dimensional semiconductor/polymer interfaces [135], except that in hybrid perovskites functional dipoles are distributed throughout the bulk of the sample. Further computational studies using described experimental data as a feedback are necessary to refine microscopic understanding of photophysics of hybrid perovskites.

To conclude, the measured Hall effect in hybrid (organo-inorganic) perovskites films and single crystals allowed to find Hall mobilities ranging from 0.5 to 60 $cm^2 V^{-1} s^{-1}$, depending on the sample composition and crystallinity. Concurrent measurements of steady-state photoconductivity and Hall carrier density allowed to directly determine bimolecular recombination coefficients (as low as ~ 10^{-10}–10^{-11}), carrier lifetimes (up to 30 μs and 2.7 ms in films and crystals, respectively) and diffusion lengths (up to 23 μm and 650 μm in films and crystals, respectively). These measurements provide the direct and conclusive evidence of a strong suppression of *e–h* recombination and remarkably weak trapping in hybrid perovskites. They show that photophysical properties of these materials are very different from those of conventional organic (such as P3HT or PTB7 conjugated polymers, used in organic PV) or inorganic semiconductors (such as c-Si or GaAs). One should emphasize that the study determines these important transport parameters directly, from steady-state transport measurements, relevant to practical applications. Dipolar polaron model has been introduced, that can help explaining the observed relatively low intrinsic carrier mobilities and drastically reduced charge recombination and trapping.

4.8. Degradation effects in perovskites

The problem of degradation of solar cells on the basis of organic-inorganic perovskites is very acute in two respects. First, as any salt, the interaction with water is very essential here. Second, lattice ionicity and great value of Madelung energy opens special ways of running the photo-chemical reactions. Let us briefly consider these particular qualities. At present a hypothetical scheme of how moisture influences perovskite decomposition has been clarified (see Fig. 20).

It is seen that when one molecule of water interacts with *n*-"molecules" of perovskite for several successive steps the disengagement of one molecule of water and one molecule of PbJ_2 takes place. This scheme goes back to the mechanism of Grotthuss [130] so that along the path of the full reaction the molecules of HJ and CH_3NH_2 are disengaged. Evidently, until now it has not been found how a perovskite composition should be changed for degradation under water to be reduced both in the presence and in the absence of material photoexcitement (evidently, the methods of quantum chemistry of solid will be useful here).

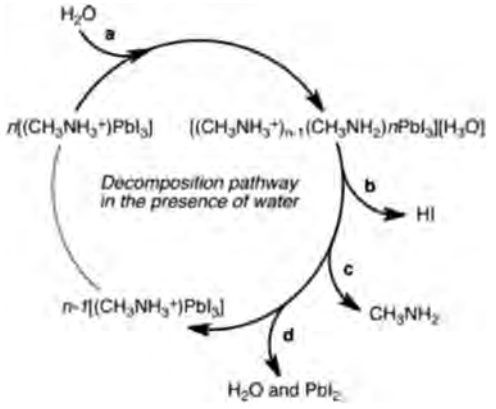

Fig. 20. Possible decomposition pathway of hybrid halide perovskites in the presence of water. One water molecule is required to initiate this process, with the decomposition being driven by the phase changes of both hydrogen iodide (soluble in water) and the methylammonia (both volatile and soluble in water) (reprinted from [33]).

It is necessary, however, to have in view that there are other (without moisture) channels of perovskite degradation under action of radiation. One of such ways is indicated by Schoonman in [131] who supposes that after hole generation at the iodide ion this hole migrates to the surface where the reaction of neutral iodide with one of the surface negative iodine ions takes place. This position is an origin of the whole consequence of reactions; as a result, degradation of perovskite structure takes place. However, analysis of this scheme does not take into account an extremely important moment: delocalization of hole that is a neutral iodine atom in the zone scheme prevents the reaction between neutral iodine and negatively charged iodine ion from running. This circumstance requires special analysis (namely, resolving the Dexter-Varley paradox); it is clearly manifested in the problems of near-threshold formation of defects and studied beginning with the late 50-s of the XX century. In our recent work on ionization-stimulated degradation of perovskite this problem was studied in detail (Oksengendler et al. [132]). Indeed (Fig. 21), if a photon knocks an electron out of any node atom of the iodine ion that means simultaneous manifestation of two circumstances; first, according to the zone structure, iodine ionization means hole appearance in the valence zone; second, from the view point of crystal chemistry, iodine neutralization immediately leads to liquidation of a potential Madelung well for iodine (the depth of this well was calculated earlier and given in Table 3). After liquidation of the Madelung well the neutral atom of iodine is on the top of the crystalline potential and tries to move to a neighboring internode.

This takes time $\tau_+ \approx 5\cdot10^{-14}$ s. However, the hole is localized at the node also for finite time τ_e. If τ_e is much less than τ_+ then, according to Dexter, the iodine atom is not shifted to the internode and there will be no defect formation (degradation). However, the situation is much more complicated: hole motion is a quantum process, which means the existence of both faster and slower cases of hole delocalization (since τ_e is the average value). Therefore, for the probability of iodine atom shifting to the internode to be defined, in spite of competition of hole delocalization, a quantum calculation should be made. That gives for the probability of internode ion shifting a magnitude $\eta = \exp(-\tau_+/\tau_e)$. It is possible to estimate the value of τ_e with the uncertainty principle $\tau_e = h/\Delta E_v$, where ΔE_v is the width of the valent zone formed by the P-states of iodine. For the parameters of perovskite $(CH_3 - NH_3)PbJ_3$ a characteristic value of the probability of iodine atom shifting to an internode is $\eta \approx 10^{-4}$, which means after iodine ion ionization the shift of one of 10,000 ionizations – that defines degradability of crystal. It is evident that all the Schoonman scheme is lowered by this factor of such an order.

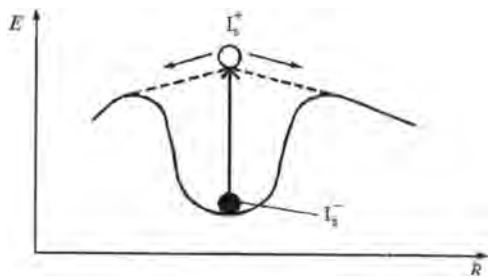

Fig. 21. The formation of dynamic Coulomb instability in the I-sublattice of perovskite (reprinted from [132]).

5. Carbon nanotubes and graphene as stable electrodes in perovskite devices

Carbon is most inert material in nature, and it is non-reactive with many ions till very high temperatures. Although carbon can be doped by iodine ions, doping may play not detrimental role, but actually improve electrical properties of nanocarbons, which we will describe below.

In present section we demonstrate that using a combination of SWCNT and MWCNT both laminated on top of the ETL of the perovskite solar cells can solve a problem of top cathode and can be used instead of Al or Ag in perovskite. This is particularly important the same most metallic electrodes to iodine containing perovskite are chemically reactive with I ions and which diffuse in under illumination and open circuit voltage (V_{oc}) increased.

5.1. Optical and electrical properties of CNT free standing sheets: MWNT vs SWCNT

CNT sheets self-assembled into optically transparent aerogels and films by dry-spinning from CNT vertically grown forests have proven to be excellent charge collectors in OPV and OLED [136]. We will briefly describe below how their Transparency can be increased simultaneously with their conductivity (usually measured as sheet resistance R_{sh} of thin film electrodes).

Thick conductor has low sheet resistance and low transmittance. Transmittance increases when the conductor became thinner, but is lose the ability of charge transportation. This tendency might be illustrated on transmittance-resistance chart: all typical conductors have a positive slope (Fig. 22) [137].

MWCNT aerogel work oppositely. MWCNT have unique ability to increase conductivity and transmittance simultaneously.

MWCNT aerogel is spinned from the forest by the Van Der Vaals force. CNT forest is grown from Si wafer by CVD process (Fig. 23a). MWCNT are mechanically strong and self-supported. Those allow to organize MWCNT as oriented flexible free-standing sheet. Initial transmittance and conductivity are not so high 50–60% on 550 nm; 300–1000 Ω/s (Fig. 23b).

MWCNT sheet densifies in IPA vapor: thin wires stick to bundles and perform holes for light percolation (Fig. 23c). This process increases transmittance without enhancement of sheet resistance, because cross section of MWCNT sheet does not change. In order to improve conductivity several strategies might be applied.

Conductivity can be enhanced by increasing cross section of conductive material. For this strategy high conductive material is deposited on MWCNT sheet. Long and thin silver nanowires **(AgNW)** twine around MWCNT bundles decreasing the overall sheet resistance. This mechanism normally combines with densification in IPA. AgNW in IPA are sprayed over MWCNT sheet. As more AgNWs solution is spray coated onto the aerogel, more apertures are formed and more silver nanowires are deposited increasing the transmittance and decreasing the sheet resistance at once.

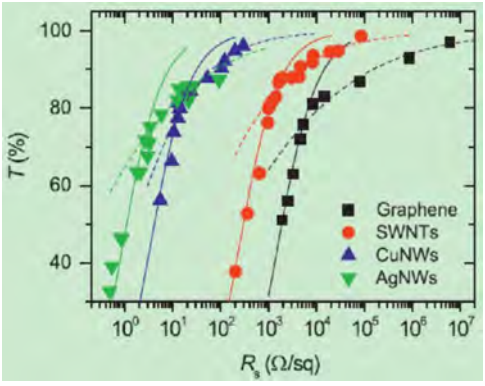

Fig. 22. Typical graph of transmittance (generally measured at 550 nm) plotted versus sheet resistance for thin films of nanostructured materials [137].

Another strategy is doping of both single wall (SWCNT) and MWCNT. Auric chloride in ethanol are sprayed in MWCNT sheet. Small particles do not have contact as AgNW. Electrons inject to CNT due to reduction of gold ($Au^{+3} \rightarrow Au^0$) on surface of carbon and increase charges mobility of CNT. This step also combines with densification of MWCNT as well.

For this moment these techniques allow to reach up to 8 Ω/sq and transparency over 95%.

5.2. Carbon nanotube as top charge collector in semitransparent perovskite solar cells

Carbon nanotubes (CNT) both single-wall (SWCNT) and multi-wall (MWCNT) have been used in the past as transparent flexible electrodes in OPV and in organic light-emitting diodes (OLEDs) as substitute for brittle indium tin oxide (ITO) [136]. They have many benefits as compared to ITO, such as possible dry processing by simple lamination. We have shown that dry drawn CNT sheets can be easily obtained in free standing films state and can be laminated either on glass as usual as anodes of OPV and OLED or if laminated on top, as cathodes collecting electrons [138]. For cathodes in OPV, the CNT should be properly doped in order to lower the work function or raise the Fermi level. We demonstrated that ionic gating is the effective way to convert CNT anodes (large work function) to low work function cathodes and the tunable OPV solar cells have been created with ionic liquids in their architecture [139]. Moreover, the tandem of OPV which are tuned by ionic gating via a common cathode have been demonstrated. Recent fast progress of hybrid perovskite solar cells in planar configuration and mesoscopic DSSC style structures, created an urgent need for effective semitransparent charge collector that can be used in tandems of perovskite solar cells with conventional Si type photovoltaic cells or thin films. Although several approaches to solve this task have been reported by using graphene or these carbon nanosheets, the top laminated perovskite solar cells with a CNT cathode has not been demonstrated. Due to ionic nature of perovskite,

$MAPbI_3$, the use of ionic liquids similar to ionic gating of our samples has failed since the perovskite was dissolved by ionic charging.

Perovskite photovoltaic planar structures look similar to organic photovoltaic **(OPV)** solar cells in the sequence of photoactive hole transport layer and electron transport layer **(ETL)**, however there is significant difference. It seems that due to large diffusion length and big concentration of carriers, there is no need for strong internal electrical field. It is created by asymmetry of electrodes like in dye-sensitized solar cells **(DSSC)**. Therefore, the work function of a cathode top electrode does not play important role in perovskite photovoltaic devices, and therefore CNT with large enough work function still can serve as top cathode, instead of chemically unstable Al, Ag or even Au.

As well known, the low stability is one of major problems of perovskite solar cells. If the environmental instability, caused by humidity of air and oxygen can be lower ease by proper encapsulation, the chemical instability of metallic electrodes is a more complicated problem. Both top Ag and Al anodes react with iodine ions, which move towards cathode upon photo illumination. It has been recently shown that Cu top cathode is much more stable as compared to Ag, Al or Au. Cu reacts with I forming CuI which is not harmful for perovskite solar cells.

Carbon is among most chemically inert elements, and particularly CNT are extremely stable in different environments. Only at high temperature above 500 °C, CNT may react with I_2 and our experiments with nanoenergetic powders with released I_2 gas inside CNT yarns showed that CNT do not react with iodine. Therefore one of motivations of this work is to check the stability of top-laminated CNT of both SWCNT and MWCNT in perovskite solar cells, at photo illumination as compared to Al cathode.

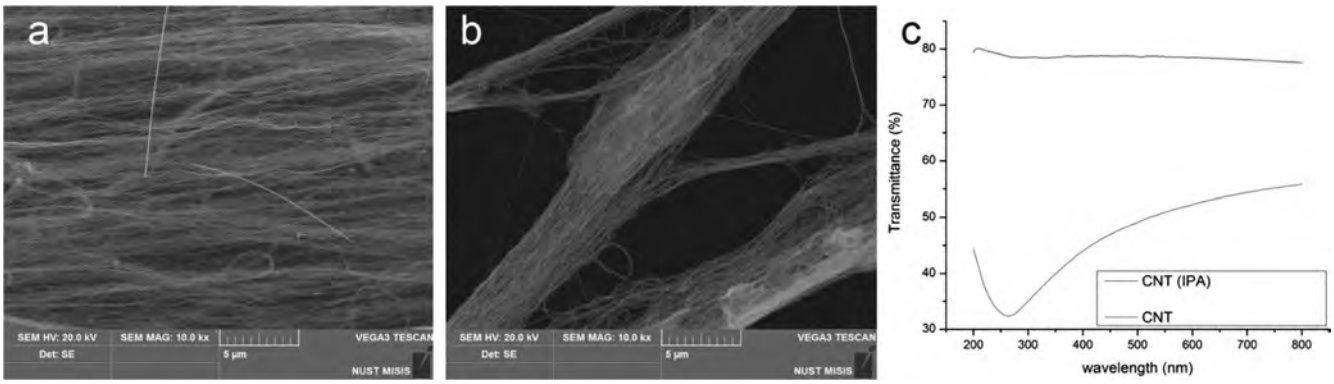

Fig. 23. SEM images of MWCNT aerogel before (a) and after densification (c), spectra of transmittance for initial and densified MWCNT.

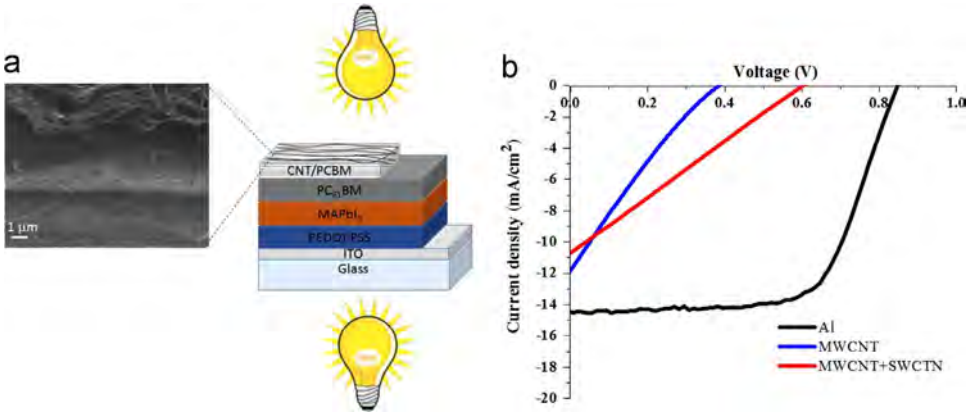

Fig. 24. (a) Schematic of the perovskite solar cell with the semitransparent CNT composite electrode. The illumination direction of the solar cell may be reversed. (b) *J–V* curve of the perovskite solar cells with reference electrode (aluminum), semitransparent top electrode with MWCNT and the CNT electrode with SWCNT incorporated.

Fig. 24 shows the scheme of the perovskite solar cell with CNT composite electrode where SWCNT, MWCNT and $PC_{61}Bm$ were deposited in that sequence. SEM image indicates that SWCNT and MWCNT are connected by a thin film of $PC_{61}BM$. The *J–V* curve for the perovskite solar cell with MWCNT electrode is shows in Fig. 25. The decrease of main parameters power conversion efficiency **(PCE)**, short-circuit current density (J_{sc}), V_{oc} and fill factor **(FF)** of perovskite solar cells with MWCNT, as compared to reference solar cell with Al top cathode is observed, however the solar cell with the CNT is clearly more stable. When SWCNT were added to the MWCNT electrode, the *Voc* increased considerably from 0.381 V to 0.608 V, while the change in *Jsc* and FF was small, resulting in an increase of the PCE from 0.98% to 1.6% with the combination of CNTs. Due to the performance improved of the perovskite solar cell with CNT composite, we change the order of the CNTs deposited and verify the behavior of the solar cells, Fig. 25.

The solar cells were illuminated on both sides. Although the PCE was higher with the incident light in the ITO side, it was demonstrated that there is good photovoltaic response through the CNTs side illuminated. The CNTs in these cells were only densified with HFE. Moreover, when $PC_{61}BM$ was added to the CNTs composite, all the parameters improved as can be seen in Fig. 25. In these cases, the $PC_{61}BM$ enhance the contact between the CNTs and the ETL of the perovskite solar cell improving the electrical contact, while the HFE only densify the CNTs and do not affect the electrical contact. The solar cell with SWCNT+MWCNT shows higher voltage and current than the solar cell with MWCNT+SWCNT after $PC_{61}BM$ added.

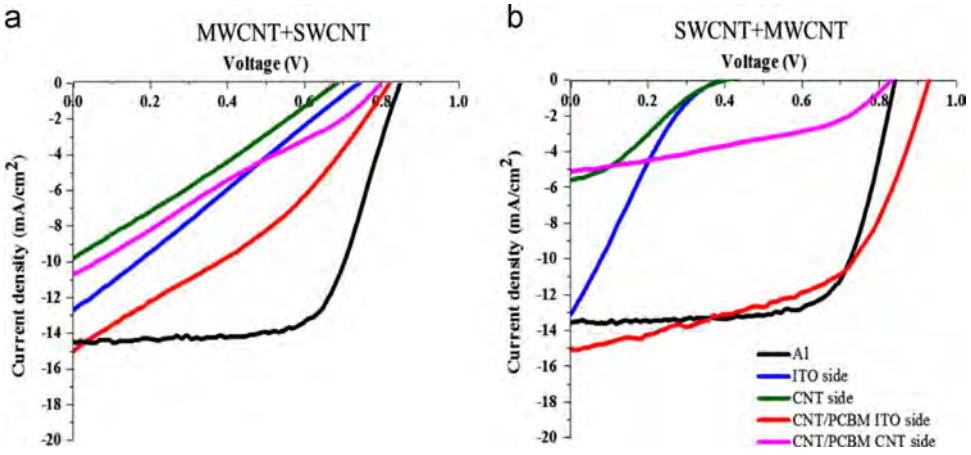

Fig. 25. *J–V* curve of the perovskite solar cell with (A) MWCNT+SWCNT and (B) SWCNT+MWCNT measured with the incident light through both sides of the device and with PCBM added.

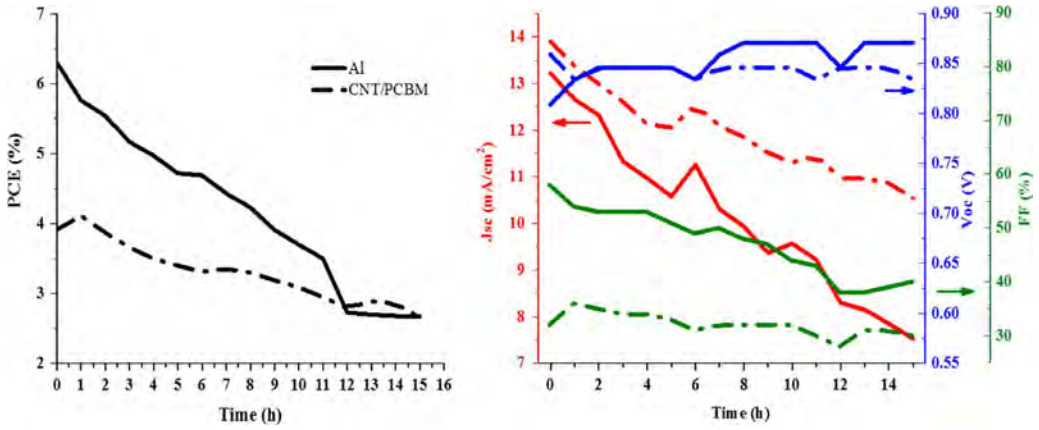

Fig. 26. Stability of the perovskite solar cells with aluminum electrode and with the CNT/PCBM composite electrode in nitrogen atmosphere at room temperature under constant illumination. Solid line indicate the solar cell with Al electrode and dashed line indicate the solar cell with CNT/PCBM composite electrode.

The stability test can be seen at Fig. 26. Below constant illumination of perovskite solar cells with Al and CNT/PCBM top cathode, some dramatic changes in the first hour were observed. The performance of both solar cells decreased under illumination, however it was faster with the Al cathode, demonstrating more stability with the CNT composite electrode. Doping of CNT by I ions coming from perovskite layer might be responsible for increased FF, which gives raise of PCE within one hour after photoillumination, as have been demonstrated that I doing improved the conductivity of CNT.

Summarizing this part we demonstrated that CNT can be used in a perovskite solar cell with semitransparent electrode which consist in SWCNT+MWCNT/PCBM and was compared with an aluminum cathode. The solar cell with the CNT composite electrode resulted in a more stable option and comparable performance with regards to metal electrode. Also, these semitransparent PV cells have the advantage that they can be illuminated from both sides.

5.3. CNT as anodes in inverted perovskite solar cells

One of the main challenge for perovskite solar cell commercialization along with stability a is relatively high production costs in comparison to conventional energy source. Perovskite industrial production consists of mainly cheap process such as roll-to-roll printing, spin-coating, doctor blading and so on. The most expensive process is vacuum evaporation of gold top electrode. Vacuum process does not match with continuous roll-to-rool process and requires complex and time consumable operations. All these create major restriction for industrial production of perovskite solar cell. Usage of semitransparent CNT aerogel is viable alternative for perovskite industrial fabrication.

Above-mentioned, CNT aerogel is flexible semitransparent conductive material. It is also mechanically strong and flexible. Moreover, transmittance allows to use it for tandem photovoltaic devices as interlayer, when light comes through CNT to photoactive layer (Fig. 27).

As of the date of this report, pristine SWCNT, with transmittance around 60%, demonstrated relative efficiency 80% regarding convectional gold electrode.

Mesoscopic perovskite solar cell was assembled as illustrated in Fig. 28. Perovskite $MAPbI_3$ photoactive layer was deposited on nanocrystalline mesoporous titan dioxide blocking layer. Spiro-OMeTAD was deposited on top of Perovskite as hole transport material. Two pixels were coated with gold by thermo-evaporation technique as reference. Two another pixels were coated with SWCNT (T_{550nm}=60%) and densified with an additional droplet of spiro-OMeTAD.

The record cell with SWCNT as electrode demonstrated 11,13% PCE against 13,88% for reference cell with conventional gold electrode

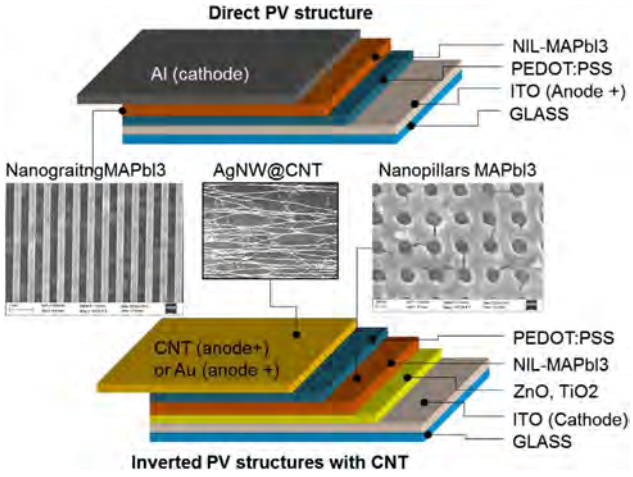

Fig. 27. (A) Direct NIL- PV and (b) Inverted NIL-PV structures. Insert 1 show the SEM image of actually created nanoimprinted MAPbI3 photoactive layers which will be used in NIL-PV. Inset 2 shows the SEM of highly transparent AgNW@CNT electrodes that will be used as charge collector.

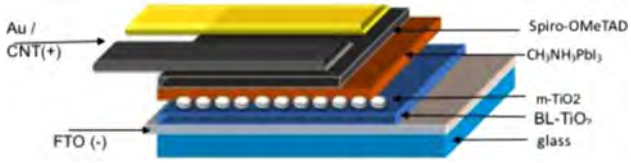

Fig. 28. Perovskite mesoscopic solar cell structure.

(Fig. 29). This cell was tested when light irradiated through SWCNT, PCE was 4,00%.

6. Conclusions

One cannot but agree with the statements of Snaith that the reason for delayed development of alternative power engineering is untimely discovery of peroskite scopes.

The record-breaking conversion parameters of the perovskite-based solar cells can be reachable for two alternative architectures of cells, mesoporous and planar, owing to the perfect semiconductor characteristics of perovskite (small band gap, high coefficient of solar radiation absorption, large diffusion length of charge carriers, direct-zone conductor, balance between electron mobility and hole one *etc.*).

The survey elucidates the methods of synthesis of perovskites, their crystalline forms (α, β, σ), types and sizes of components ABX_3 and their effect on electronic structure and energy levels, as well as special

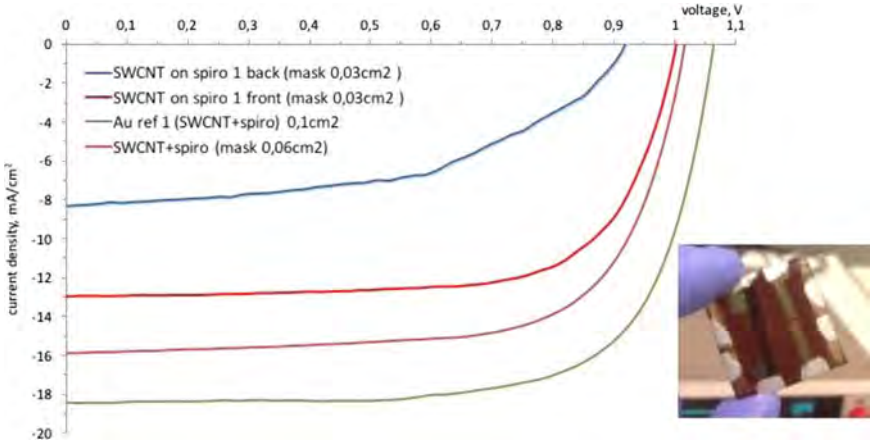

Fig. 29. IV curve of mesoscopic perovskite solar cell with gold and SWCNT top electrodes. This result demonstrates advantaches of CNT as alternative of conventional gold electrode.

features of crystallization, including nucleation and growth of crystallites and ways of their regulation.

Realization of the necessary characteristics in cells directly depends on quality of formed perovskite film (uniformity, absence of pores, high degree of crystallinity and substrate coverage, optimal sizes of crystallites). Briefly, consideration has been given to almost all the available methods of film manufacturing with indication of disadvantages and advantages of each of them, as well as to numerous ways of optimization of formation and crystallization of perovskites (precursor relation, thermal annealing, annealing with solvent, addition introducing *etc.*).

The important stages (transition from solar cells on the basis of dyes with electrolyte with replacement of the latter by solid HTM and further replacement of dyes by perovskites, ambipolarity of perovskites and nature of defects in them, progressive methods of solar cell formation, possible channels of recombination of charge carriers and ways of their weakening *etc.*) of development of the studies in this direction which defined the impetuous growth (for 2–3 years) in the power conversion efficiency from 3% to 20% have been considered. A list of used ETM and HTM and the principles of their selection depending on cell architecture has been presented.

Nevertheless, the optimization approaches for strengthening the conversion efficiency of cells cannot be applied in full because of the absence of a definite mechanism of operation of photovoltaic devices on the basis of perovskites. The following experimental facts should be noted as the main reasons.

Undoubtedly, perovskites are excellent absorbers of solar radiation. However, it is not quite clear how the free carriers of charges are generated.

Initially generation of free carriers of charges in perovskites was inclined to the exciton nature and in recent time, as a result of the exact estimations of binding energy of the electron-hole pair and dielectric constant, this process is mainly associated with the fact that the photoexcitation similar to inorganic semiconductors is spontaneously completed by dissociation into free carriers.

A question connected with hysteresis in real perovskite-based cells which differently depends on cell architecture remains open. The reason for this phenomenon is seen in high capacity at low frequencies (greatly differed values of dielectric constant on frequency) inducing the polarization of an organic component of the perovskite and their migration, as well as the formation of non-controlled defects at boundaries. At the same time, there are data that if the cell components are chosen appropriately it is possible to reach the absence of hysteresis for a standard n-i-p structure. A role of chlorine in the perovskite film providing high values of diffusion length of charges more than μm and conversion efficiency is not quite clear. Despite of the opinion about a role of the chlorine atoms in formation of qualitative films it is necessary to continue these studies for all the determining factors to be completely revealed to make a necessary quality of films.

Toxicity of lead containing in perovskite also causes some problems. Its replacement by tin, prima facie, is principally possible, however its light oxidization $Sn^{+2} \rightarrow Sn^{+4}$ requires further studies and appropriate decisions.

Operation stability of cells in the environment of oxygen and moisture, UV-light and temperature is also an important problem.

Among many directions to which the theoretical studies of organic-inorganic perovskites were devoted only some of them, most important to our mind, were elucidated in this survey. The computational calculations of Madelung energy for each position of the ABX_3 lattice (where A^+ is the organic ions, B^{2+} is the metallic ions, X is the haloid ions) have been considered and it has been shown that these energies are sufficiently high. The latter circumstance is important for the process of degradation.

The issues of calculating the perovskite electronic structure on the basis of first principles with DFT and its modifications accent attention to a value of the band gap, which is very important for photochemical reactions.

Serious attention has been paid to the problem of own defects with swallow, resonance and deep levels in the electronic spectra of perovskites. It is noted that the own defects with the least energy have no deep states in the band gap; it is also noted that there is an indication to specific defects with U-negative properties.

Further, the problem of chlorine in perovskite $MAPbJ_{3-x}Cl_x$ has been considered. As an alternative to the available approaches, an idea about electronic spectra reconfiguration in these mixed crystals as a result of the quasi-chemical reaction $Cl_S+J_i \rightarrow [Cl_SJ_i]$ has been proposed. Its efficiency is due to different dilatation signs of charges of atomic chlorine and internodal ion. It has been mentioned that it is possible to explain a simultaneous decrease in charge carrier scattering and liquidation of a deep trap formed by internodal iodine.

The variants of interpreting the experiments on dynamics of charge carrier recombination (made by the group of Prof. Dyakonov in 2015) have been discussed in detail. Several models: hemin recombination of Onsager (its non-stationary variant), three-particle recombination (on the basis of the approaches of Dj. Dj. Tomson and Shockley-Read-Hall), polarization model of separating the paths of charge carrier motion (Frost with combination of the approach of Onsager Mazumder) have been considered. A conclusion has been made that more attractive is a model of three-particle recombination (with consideration of attachment level).

Finally, the models of degradation (both under moisture and as a result of radiation ionization) have been considered in very detail. The role of Dexter–Varley paradox (competition process of J_S^0 state mixing and hole delocalization in the valence zone) is considered as very

important. The latter circumstance can radically change the ideas about the efficiency of photochemical reactions. In view of that, it should be noted that the estimation of the degradation efficiency towards its increase can be influenced by the existence of such charge carriers as polarons. Extremely important and requiring special mentioning is physics and chemistry of defects in organic-inorganic perovskites. With a very great degree of generalization, it should be considered that this aspect is a crossroad of crystal chemistry, technology, optics, electronics, magnetochemistry and others, naturally including the problem of degradation of this class of materials. Note that the latter aspect proved to be rich in special features of photochemical reactions. Moreover, it is unusually perspective from the view point of irradiation of multicomponent media with high-energy radiation. Indeed, in view of this aspect, great perspectives in radiation technology of such a class of solar cells are open, as well as in cosmonautics as being principally important for application. All the above stated, with great reliability, allows prediction of great future for organic-inorganic perovskites in science and engineering.

The excellent surveys published in recent time reflect not only the state and problems but also sound hopes that the future of alternative sources of energy is in solar cells on the basis of perovskites.

Acknowledgements

Support for this work was provided from the Ministry of Education and Science of the Russian Federation in the framework of Increase Competitiveness Program of NUST “MISiS” (No. K2-2015-014). We also appreciate the partial support of Welch Foundation grant AT 16–17 and CONACYT for academic opportunities and academic support.

References

[1] D.B. Mitzi, Solution-processed inorganic semiconductors, J. Mater. Chem. 14 (2004) 2355–2365. http://dx.doi.org/10.1039/B403482A.
[2] D.B. Mitzi, K. Chondroudis, C.R. Kagan, Organic–inorganic electronics, J. Res. Dev. 45 (1) (2001) 29–45. http://dx.doi.org/10.1147/rd.451.0029.
[3] D.B. Mitzi, S. Wang, C.A. Feild, C.A. Chess, A.M. Guloy, Containing (110)-oriented perovskite sheets, Science 267 (1995) 1473–1476. http://dx.doi.org/10.1126/science.267.5203.1473.
[4] D.B. Mitzi, Synthesis, structure, and properties of organic–inorganic perovskites and related materials, Prog. Inorg. Chem. 48 (2007) 1–121. http://dx.doi.org/10.1002/9780470166499.ch1.
[5] C.R. Kagan, D.B. Mitzi, C.D. Dimitrakopoulos, Organic–inorganic hybrid materials as semiconducting channels in thin-film field-effect transistors, Science 286 (1999) 945–947. http://dx.doi.org/10.1126/science.286.5441.945.
[6] C.C. Stoumpos, C.D. Mallinkas, M.G. Kanatzidis, Semiconducting tin and lead iodide perovskites with organic cations: phase transitions, high mobilities, and near-infrared photoluminescent properties, Inorg. Chem. 52 (15) (2013) 9019–9038. http://dx.doi.org/10.1021/ic401215x.
[7] A. Kojima, M. Ikogami, K. Teshima, T. Miyasaka, Highly luminescent lead bromide perovskite nanoparticles synthesize with porous alumina media, Chem. Lett. 41 (4) (2012) 397–399. http://dx.doi.org/10.1246/cl.2012.397.
[8] A. Kojima, K. Teshima, T. Miyasaka, Y. Shirai, Novel photoelectrochemical cell with mesoscopic electrodes sensitized by lead-halide compounds. in 2Proceedings of the 10th ECS Meeting (ECS, 2006), p. 397.
[9] A. Kojima, K. Teshima, Y. Shirai, T. Miyasaka, Organometal halide perovskites as visible-light sensitizers for photovoltaic cells, J. Am. Chem. Soc. 131 (17) (2009) 6050–6051. http://dx.doi.org/10.1021/ja809598r.
[10] J.H. Im, C.R. Lee, J.W. Park, N.G. Park, 6.5% efficient perovskite quantum-dot-sensitized solar cell, Nanoscale 3 (2011) 4088–4093. http://dx.doi.org/10.1039/C1NR10867K [Communication].
[11] I. Robel, V. Subramanian, M. Kuno, P.V. Kamat, Quantum dot solar cells. Harvesting light energy with CdSe nanocrystals molecularly linked to mesoscopic TiO_2 films, J. Am. Chem. Soc. 128 (2006) 2385–2393. http://dx.doi.org/10.1021/ja056494n.
[12] J.B. Sambur, T. Novet, B.A. Parkinson, Multiple exciton collection in a sensitized photovoltaic system, Science 330 (2010) 63–66. http://dx.doi.org/10.1126/science.1191462.
[13] A. Zaban, O.I. Mićić, B.A. Gregg, A.J. Nozik, Photosensitization of Nanoporous TiO2 Electrodes with InP Quantum Dots 14, Langmuir, 1998, pp. 3153–3156. http://dx.doi.org/10.1021/la9713863.
[14] P. Yu, K. Zhu, A.G. Norman, S. Ferrere, A.J. Frank, A.J. Nozik, Nanocrystalline TiO_2 solar cells sensitized with InAs quantum dots, J. Phys. Chem. B 110 (2006) 25451–25454. http://dx.doi.org/10.1021/jp064817b.
[15] S.J. Moon, Y. Itzhaik, J.-H. Yum, S.M. Zakeeruddin, G. Hodes, M. Gra¨tzel, Sb_2S_3-based mesoscopic solar cell using an organic hole conductor, J. Phys. Chem. Lett. 1 (2010) 1524–1527. http://dx.doi.org/10.1021/jz100308.
[16] H.-S. Kim, C.-R. Lee, J.-H. Im, K.-B. Lee, T. Moehl, A. Marchioro, S.-J. Moon, R. Humphry-Baker, J.-H. Yum, J.E. Moser, M. Gratzel, N.-G. Park, Lead iodide perovskite sensitized all-solid-state submicron thin film mesoscopic solar cell with efficiency exceeding 9%, Sci. Rep. 2 (2012), article number: 591. http://dx.doi.org/10.1038/srep00591.
[17] L. Etgar, P. GaO, Z. Xue, Q. Peng, A.K. Chandirun, B. Liu, Md.K. Nazeeruddin, M. Grätzel, Mesoscopic $CH_3NH_3PbI_3/TiO_2$ heterojunction solar cells, J. Am. Chem. Soc. 134 (42) (2012) 17396–17399. http://dx.doi.org/10.1021/ja307789s.
[18] M.M. Lee, J. Teuscher, T. Miyasaka, T.N. Murakami, H.J. Snaith, Efficient hybrid solar cells based on meso-superstructured organometal halide perovskites, Science 338 (2012) 643–647. http://dx.doi.org/10.1126/science.1228604.
[19] S. Stranks, G.E. Eperon, G. Grancini, C. Menelaou, M.J.P. Alcocer, T. Leytens, L. Herz, A. Petrozza, H.J. Snaith, Electron-hole diffusion lengths exceeding 1 μm in an organometal trihalide perovskite absorber, Science 342 (2013) 341–343. http://dx.doi.org/10.1126/science.1243982.
[20] J. Burschka, N. Pellet, S.-J. Moon, K.H. Baker, P. GaO, M.K. Nazeeruddin, M. Grätzel, Sequential deposition as a route to high-performance perovskite-sensitized solar cells, Nature 499 (2013) 316–319. http://dx.doi.org/10.1038/nature12340.
[21] J. Burschka, High Performance Solid-state Mesoscopic Solar Cells [Ph.D.Thesis], École Polytechnique Fédérale de Lausanne, Suisse, 2013, p. 145.
[22] M. Liu, M.B. Johnston, H.J. Snaith, Efficient planar heterojunction perovskite solar cells by vapour deposition, Nature 501 (2013) 395–398. http://dx.doi.org/10.1038/nature12509.
[23] Q. Chen, H. Zhou, Z. Hong, S. LuO, H.-Sh Duan, H.-H. Wang, Y. Liu, G.- Li, Y. Yang, Planar heterojunction perovskite solar cells via vapor-assisted solution process, J. Am. Chem. Soc. 136 (2) (2014) 622–625. http://dx.doi.org/10.1021/ja411509g.
[24] Y. Zhao, K. Zhu, Three-step sequential solution deposition of PbI_2-free $CH_3NH_3PbI_3$ perovskite, J. Mater. Chem. A 3 (17) (2015) 9086–9091. http://dx.doi.org/10.1039/C4TA05384B.
[25] J.T.W. Wang, J.M. Ball, E.M. Barea, A. Abate, J.A. Alexander-Webber, J. Huang, M. Saliba, I. Mora-Sero, J. Biqueret, H.J. Snaith, K.J. Nicholas, Low-temperature processed electron collection layers of graphene/TiO_2 nanocomposites in thin film perovskite solar cells, Nano Lett. 14 (2) (2014) 724–730. http://dx.doi.org/10.1021/nl403997a.
[26] K. Wojciechowski, M. Saliba, T. Leijtens, A. Abate, H.J. Snaith, Sub-150 °C processed meso-superstructured perovskite solar cells with enhanced efficiency, Energy Environ. Sci. 7 (3) (2014) 1142–1147. http://dx.doi.org/10.1039/C3EE43707H.
[27] S. Ryu, J.H. Noh, N.J. Jeon, Y. Chan Kim, W.S. Yang, J. Seo, S.I. Seok, Voltage output of efficient perovskite solar cells with high open-circuit voltage and fill factor, Energy Environ. Sci. 7 (2014) 2614–2618. http://dx.doi.org/10.1039/C4EE00762J.
[28] N.J. Jeon, J.H. Noh, Y.C. Kim, W.S. Yang, S. Ryu, S.I. Seok, Solvent engineering for high-performance inorganic–organic hybrid perovskite solar cells, Nat. Mater. 13 (2014) 897–903. http://dx.doi.org/10.1038/nmat4014.
[29] N.J. Jeon, H.G. Lee, Y.C. Kim, J. Seo, J.H. Noh, J. Lee, S.I. Seok, o-Methoxy substituents in spiro-OMeTAD for efficient inorganic-organic hybrid perovskite solar cells, Chem. Soc. 136 (22) (2014) 7837–7840. http://dx.doi.org/10.1021/ja502824c.
[30] H. Zhou, Q. Chen, G. Li, S. Luo, T.B. Song, H.S. Duan, Z. Hong, J. You, Y. Liu, Y. Yang, Photovoltaics. Interface engineering of highly efficient perovskite solar cells, Science 345 (6196) (2014) 542–546. http://dx.doi.org/10.1126/science.1254050.
[31] H.J. Snaith, Perovskites: the emergence of a new era for low-cost, high-efficiency solar cells, J. Phys. Chem. Lett. 4 (21) (2013) 3623–3630. http://dx.doi.org/10.1021/jz4020162.
[32] K. Leo, Perovskite photovoltaics: signs of stability, Nat. Nanotechnol. 10 (2015) 574–575. http://dx.doi.org/10.1038/nnano.2015.139.
[33] J.M. Frost, K.T. Butler, F. Brivio, Ch.H. Hendon, M. van Schilfgaarde, A. Walsh, Atomistic origins of high-performance in hybrid halide perovskite solar cells, Nano Lett. 14 (5) (2014) 2584–2590. http://dx.doi.org/10.1021/nl500390f.
[34] W.-J. Yin, T. Shi, Y. Yan, Unique properties of halide perovskites as possible origins of the superior solar cell performance, Adv. Mater. 26 (2014) 4653–4658. http://dx.doi.org/10.1002/adma.201306281.
[35] B. Lee, Y. Chen, D. Fu, H.T. Yi, K. Czelen, H. Najafov, V. Podzorov, Trap healing and ultralow-noise Hall effect at the surface of organic semiconductors, Nat. Mater. 12 (2013) 1125–1129. http://dx.doi.org/10.1038/nmat3781.
[36] Chen, H.T. Yi, X. Wu, R. Haroldson, Y.N. Gartstein, Y.I. Rodionov, K.S. Tikhonov, A. Zakhidov, X.-Y. Zhu, V. Podzorov, Extended carrier lifetimes and diffusion in hybrid perovskites revealed by Hall effect and photoconductivity measurements, Nat. Commun. 7 (2016), article number: 12253. http://dx.doi.org/10.1038/ncomms12253.
[37] H. Wang, L. Valkunas, T. Cao, L. Whittaker-Brooks, G.R. Fleming, Coulomb screening and coherent phonon in methylammonium lead iodide perovskites, J. Phys. Chem. Lett. 7 (16) (2016) 3284–3289. http://dx.doi.org/10.1021/acs.jpclett.6b01425.
[38] C. Wehrenfennig, G.E. Eperon, M.B. Johnston, H.J. Snaith, L.M. Herz, High charge carrier mobilities and lifetimes in organolead trihalide perovskites, Adv. Mater. 26 (2014) 1584–1589. http://dx.doi.org/10.1002/adma.201305172.
[39] A. Pivrikas, H. Neugebauer, N.S. Sariciftci, Charge carrier lifetime and recombination in bulk heterojunction solar cells, IEEE J. Sel. Top. Quantum Electron 16 (6) (2010) 1746–1758. http://dx.doi.org/10.1109/JSTQE.2010.2044978.
[40] H.L. Welles, Uber die Casium- und Kalium-Bleihalogenide, Sheffield Scintific

School, New Haven, Conn, 1893. http://dx.doi.org/10.1002/zaac.18930030124.
[41] D. Weber, $CH_3NH_3SnBr_{3-x}$ (x = 0-3), a Sn(II)-system with the cubic perovskite structure, Z. Naturfisch 33b (1978) 862–865.
[42] D. Weber, $CH_3NH_3PbX_3$, a Pb(II)-system with the cubic perovskite structure, Z. Naturfisch 33b (1978) 1443–1445.
[43] D.B. Mitzi, C.A. Feild, W.T.A. Harrison, A.M. Guloy, Conducting Tin halides with a layered organic-based perovskite structure, Nature 369 (1994) 467–469. http://dx.doi.org/10.1038/369467a0.
[44] D.B. Mitzi, Templating and structural engineering in organic–inorganic perovskites, J. Chem. Soc. Dalton Trans. (2001) 1–12. http://dx.doi.org/10.1039/B007070J.
[45] Z. Cheng, J. Lin, Layered organic–inorganic hybrid perovskites: structure, optical properties, film preparation, patterning and templating engineering, Cryst. Eng. Comm. 12 (2010) 2646–2662. http://dx.doi.org/10.1039/C001929A.
[46] Y.Y. Li, C.K. Lin, G.L. Zheng, Z.Y. Cheng, H. You, W.D. Wang, J. Lin, Novel < 110 > -oriented organic–inorganic perovskite compound stabilized by N-(3-Aminopropyl)imidazole with improved optical properties, Chem. Mater. 18 (2006) 3463–3469. http://dx.doi.org/10.1021/cm060714u.
[47] Y.Y. Li, G.L. Zheng, J. Lin, Synthesis, structure, and optical properties of a contorted < 110 > -oriented layered hybrid perovskite: c3h11sn3pbbr4, Eur. J. Inorg. Chem. 10 (2008) 1689–1692. http://dx.doi.org/10.1002/ejic.200700927.
[48] J. Zaleski, A. Pietraszko, Structure at 200 and 298 K and X-ray investigations of the phase transition at 242 K of $[NH_2(CH_3)_2]_3Sb_2Cl_9$ (DMACA), Acta Crystallogr vol. B52 (1996) 287–295. http://dx.doi.org/10.1107/S0108768195010615.
[49] I.N. Burmistrov, D.V. Kuznetsov, A.G. Yudin, D.S. Muratov, S.I. Milyaeva, M.A. Kostitsyn, M.V. Gorshenkov, Analysis of the effect of preparation conditions for potassium polytitanates on their morphological properties, Refract. Ind. Ceram. 52 (6) (2012) 393–397. http://dx.doi.org/10.1007/s11148-012-9437-y.
[50] F.S. Fedorov, A.S. Varezhnikov, I. Kiselev, V.V. Kolesnichenko, I.N. Burmistrov, M. Sommer, D. Fuchs, C. Kübel, A.V. Gorokhovsky, V.V. Sysoev, Potassium polytitanategas-sensor study by impedance spectroscopy, Anal. Chim. Acta 897 (2015) 81–86. http://dx.doi.org/10.1016/j.aca.2015.09.029.
[51] Xiaoyan Gan, Ou Wang, Keyong Liu, Xiangjun Du, Liling Guo, Hanxing Liu, 2D homologous organic-inorganic hybrids as light-absorbers for planer and nanorod-based perovskite solar cells, Sol. Energy Mater. Sol. Cells 162 (2017) 93–102. http://dx.doi.org/10.1016/j.solmat.2016.12.047.
[52] B. Saparov, F. Hong, J.P. Sun, H.S. Duan, W. Meng, S. Cameron, I.G. Hill, Y. Yan, D.B. Mitzi, Thin-film preparation and characterization of $Cs_3Sb_2I_9$: a lead-free layered perovskite semiconductor, Chem. Mater. 27 (2015) 5622–5632. http://dx.doi.org/10.1021/acs.chemmater.5b01989.
[53] D.H. Cao, C.C. Stoumpos, O.K. Farha, J.T. Hupp, M.G. Kanatzidis, 2D homologous perovskites as light-absorbing materials for solar cell applications, J. Am. Chem. Soc. 137 (24) (2015) 7843–7850. http://dx.doi.org/10.1021/jacs.5b03796.
[54] D. Cortecchia, H.A. Dewi, J. Yin, A. Bruno, S. Chen, T. Baikie, P.P. Boix, M. Grätzel, S. Mhaisalkar, C. Soci, Lead-free $MA_2CuCl_xBr_{4-x}$ hybrid perovskites, Inorg. Chem. 55 (2016) 1044–1052. http://dx.doi.org/10.1021/acs.inorgchem.5b01896.
[55] K. Yao, X. Wang, Y. Xu, F. Li, L. Zhou, Multilayered perovskite materials based on polymeric-ammonium cations for stable large-area solar cell, Chem. Mater. 28 (9) (2016) 3131–3138. http://dx.doi.org/10.1021/acs.chemmater.6b00711.
[56] Z. Xiao, W. Meng, B. Saparov, H.S. Duan, C. Wang, C. Feng, W.Q. Liao, W. Ke, D. Zhao, J. Wang, Photovoltaic properties of two-dimensional $(CH_3NH_3)_2Pb(SCN)_2I_2$ perovskite: a combined experimental and density-functional theory study, J. Phys. Chem. Lett. 7 (7) (2016) 1213–1218. http://dx.doi.org/10.1021/acs.jpclett.6b00248.
[57] I.C. Smith, E.T. Hoke, D. Solis-Ibarra, M.D. McGehee, H.I. Karunadasa, A. Layered, Hybrid perovskite solar-cell absorber with enhanced moisture stability, Angew. Chem. 126 (42) (2014) 11414–11417. http://dx.doi.org/10.1002/ange.201406466.
[58] S. Pang, et al., $NH_2CH{=}NH_2PbI_3$: an alternative organolead iodide perovskite sensitizer for mesoscopic solar cells, Chem. Mater. 26 (3) (2014) 1485–1491. http://dx.doi.org/10.1021/cm404006p.
[59] J.G. Bednorz, K.A. Muller, Possible high T_c superconductivity in the Ba–La–Cu–O system, Z. Phys. B. Condens. Matter 64 (1986) 189–193. http://dx.doi.org/10.1007/BF01303701.
[60] M.A. Green, A. Ho-Baillie, H.J. Snaith, The emergence of perovskite solar cells, Nat. Photonics 8 (2014) 506–514. http://dx.doi.org/10.1038/nphoton.2014.134.
[61] V.M. Goldschmidt, Die Gesetze der Krystallochemie, Naturwissenschaften 14 (21) (1926) 477–485. http://dx.doi.org/10.1007/BF01507527.
[62] G. Xing, N. Mathews, S. Sun, S.S. Lim, Y.M. Lam, M. Gratzel, S. Mhaisalkar, T.C. Sum, Long-range balanced electron- and hole-transport lengths in organic-inorganic $CH_3NH_3PbI_3$, Science 342 (2013) 344–347. http://dx.doi.org/10.1126/science.1243167.
[63] S. Sun, T. Salim, N. Mathews, M. Duchamp, C. Boothroyd, G. Xing, T.C. Sum, Y.M. Lam, The origin of high efficiency in low-temperaturesolution-processable bilayer organometal halide hybrid solar cells, Energy Environ. Sci. 7 (2014) 399–407. http://dx.doi.org/10.1039/C3EE43161D.
[64] K. Tanaka, T. Takahashi, T. Kondo, K. Umeda, K. Ema, T. Umebayashi, K. Asai, K. Uchida, N. Miura, Bandgap and exciton binding energies in lead-iodide-based natural quantum-well crystals. Part I, Jpn. J. Appl. Phys. 44 (2005) 5923–5932. http://dx.doi.org/10.1143/JJAP/44/5923.
[65] K. Tanaka, T. Takahoshi, T. Ban, T. Kando, K. Uchida, N. Miura, Comparative study on the excitons in lead-halide-based perovskite-type crystals $CH_3NH_3PbBr_3$ $CH_3NH_3PbI_3$, Solid State Commun. 127 (9-10) (2003) 619–623. http://dx.doi.org/10.1016/S0038-1098(03)00566-0.
[66] Qianqian Lin, Ardalan Armin, Ravi Chandra Raju Nagiri, Paul L. Burn, Paul Meredith, Electro-optics of perovskite solar cells, Nat. Photonics 9 (2015) 106–112. http://dx.doi.org/10.1038/nphoton.2014.284.
[67] H.-S. Kim, I. Mora-Sero, V. Gonzales-Pedro, F. Fabregat-Santiago, E.J. Juarez-Perez, N.-G. Park, J. Bisquert, Mechanism of carrier accumulation in perovskite thin-absorber solar cells, Nat. Commun. 4 (2013), Article number: 2242. http://dx.doi.org/10.1038/ncomms3242.
[68] J. Tilchin, D.N. Dirin, G.I. Maikov, A. Sashchiuk, M.V. Kovalenko, E. Lifshitz, Hydrogen-like Wannier–Mott excitons in single crystal of methylammonium lead bromide perovskite, ACS Nano 10 (6) (2016) 6363–6371. http://dx.doi.org/10.1021/acsnano.6b02734.
[69] Y. Kutes, L. Ye, Yu Zhou, Sh Pang, B.D. Huey, N.P. Padture, Direct observation of ferroelectric domains in solution-processed $CH_3NH_3PbI_3$ perovskite thin films, J. Phys. Chem. Lett. 5 (19) (2014) 3335–3339. http://dx.doi.org/10.1021/jz501697b.
[70] N. D'Innocenzo, G. Grancini, M.J.P. Alcocer, A.R.S. Kandada, S.D. Stranks, M.M. Lee, G. Launzani, H.S. Snaith, A. Petrozza, Excitons versus free charges in organo-lead tri-halide perovskites, Nat. Commiations 5 (2014), art. no. 3586. http://dx.doi.org/10.1038/ncomms4586.
[71] G. Niu, X. Guo, L. Wang, Review of recent progress in chemical stability of perovskite solar cells, J. Mater. Chem. A 3 (17) (2015) 8970–8980. http://dx.doi.org/10.1039/C4TA04994B.
[72] C. Roiland, G. Trippe-Allard, K. Jemli, B. Alonso, J.-C. Ameline, R. Gautier, T. Bataille, L. Le Polles, E. Deleporte, J. Even, C. Katan, Multinuclear NMR as a tool for studying local order and dynamics in $CH_3NH_3PbX_3$ (X = Cl, Br, I) hybrid perovskites, Phys. Chem. Chem. Phys. 18 (2016) 27133–27142. http://dx.doi.org/10.1039/C6CP02947G.
[73] H. Yu, F. Wang, F. Xie, W. Li, J. Chen, N. Zhao, The role of chlorine in the formation process of «$CH_3NH_3PbI_{3-x}Cl_x$» perovskite, Adv. Funct. Mater. 24 (2014) 7102–7108. http://dx.doi.org/10.1002/adfm.201401872.
[74] T.M. Koh, K. Fu, Y. Fang, S. Chen, T.C. Sum, N. Mathews, S.G. Mhaisalkar, P.P. Boix, T. Baikie, Formamidinium-containing metal-halide: an alternative material for near-IR absorption perovskite solar cells, J. Phys. Chem. C 118 (2013) 16458–16462. http://dx.doi.org/10.1021/jp411112k.
[75] G.E. Eperon, S.D. Stranks, C. Menelaou, M.B. Johnston, L.M. Herz, H.J. Snaith, Formamidinium lead trihalide: a broadly tunable perovskite for efficient planar heterojunction solar cells, Energy Environ. Sci. 7 (2014) 982–988. http://dx.doi.org/10.1039/C3EE43822H.
[76] N. Pellet, P. Gao, G. Gregori, T.-Y. Yang, M.K. Nazeeruddin, J. Maier, M. Grätzel, Mixed-organic-cation perovskite photovoltaics for enhanced solar-light harvesting, Angew. Chem. Int. Ed. 53 (12) (2014) 3151–3157. http://dx.doi.org/10.1002/anie.201309361.
[77] T. Salim, S. Sun, Y. Abe, A. Krishna, A.C. Grinsdebe, Y.M. Lam, Perovskite-based solar cells: impact of morphology and device architecture on device performance, J. Mater. Chem. A 3 (17) (2014) 8943–8969. http://dx.doi.org/10.1039/C4TA05226a.
[78] M.H. Kumar, N. Yantara, S. Dharani, M. Graetzel, S. Mhaisalkar, P.P. Boix, N. Mathews, Flexible, low-temperature, solution processed ZnO-based perovskite solid state solar cells, Chem. Commun. 49 (2013) 11089–11091. http://dx.doi.org/10.1039/C3CC46534A.
[79] D. Liu, T.L. Kelly, Perovskite solar cells with a planar heterojunction structure prepared using room-temperatur esolution processing techniques, Nat. Photonics 8 (2014) 133–138. http://dx.doi.org/10.1038/nphoton.2013.342.
[80] M. Graetzel, R.A.J. Janssen, D.B. Mitzi, E.H. Sargent, Materials interface engineering for solution-processed photovoltaics, Nature 488 (2012) 304–312. http://dx.doi.org/10.1038/nature11476.
[81] F.C. Krebs, Fabrication and processing of polymer solar cells: a review of printing and coating techniques, Sol. Energy Mater. Sol. Cells 93 (4) (2009) 394–412. http://dx.doi.org/10.1016/j.solmat.2008.10.004.
[82] D.A.R. Barkhouse, O. Gunawan, T. Gotmen, T.K. Todorov, D.B. Mitzi, Device characteristics of a 10.1% hydrazine-processed $Cu_2ZnSn(Se,S)_4$ solar cell, Prog. Photovolt.: Res. Appl. 20 (1) (2012) 6–11. http://dx.doi.org/10.1002/pip.1160.
[83] T.K. Todorov, O. Gunawan, T. Gokmen, D.B. Mitzi, Solution-processed Cu(In,Ga)$(S,Se)_2$ absorber yielding a 15.2% efficient solar cell, Prog. Photovolt.: Res. Appl. 21 (1) (2013) 82–87. http://dx.doi.org/10.1002/pip.1253.
[84] H.-B. Kim, H. Choi, J. Jeong, S. Kim, B. Walker, S. Song, J.Y. Kim, Mixed solvents for the optimization of morphology in solution-processed, inverted-type perovskite/fullerene hybrid solar cells, Nanoscale 6 (2014) 6679–6683. http://dx.doi.org/10.1039/C4NR00130C.
[85] M. Xiao, F. Huang, W. Huang, Y. Dkhissi, Y. Zhu, J. Etheridge, A. Gray-Weale, U. Bach, Y.-B. Cheng, L. Spiccia, A fast deposition-crystallization procedure for highly efficient lead iodide perovskite thin-film solar cells, Angew. Chem. Int. Ed. 53 (2014) 9898–9903. http://dx.doi.org/10.1002/anie.201405334.
[86] F. Huang, Y. Dkhissi, W. Huang, M. Xiao, I. Benesperi, S. Rubanov, Y. Zhu, X. Lin, L. Jiang, Y. Zhou, A. Gray-Weale, J. Etheridge, C.R. McNeill, R.A. Caruso, U. Bach, L. Spiccia, Y.-B. Cheng, Gas-assisted preparation of lead iodide perovskite films consisting of a monolayer of single crystalline grains for high efficiency planar solar cells, Nano Energy 10 (2014) 10–18. http://dx.doi.org/10.1016/j.nanoen.2014.08.015.
[87] W.-J. Yin, J.-H. Yang, J. Kang, Y. Yanb, S.-H. Wei, Halide perovskite materials for solar cells: a theoretical review. A Theoretical Review, J. Mater. Chem. A 3 (17) (2015) 8926–8942. http://dx.doi.org/10.1039/c4ta05033a.
[88] W.-J. Yin, T. Shi, Y. Yan, Unusual defect physics in $CH_3NH_3PbI_3$ perovskite solar cell absorber, Appl. Phys. Lett. 104 (6) (2014), article number: 063903. http://dx.doi.org/10.1063/1.4864778.
[89] G. Li, Y. Yao, H. Yang, V. Shrotriya, G. Yang, Y. Yang, «Solvent Annealing» Effect

in polymer solar cells based on poly(3-hexylthiophene) and methanofullerenes, Adv. Funct. Mater. 17 (10) (2007) 1636–1644. http://dx.doi.org/10.1002/adfm.200600624.
[90] Z. Xiao, Q. Dong, C. Bi, Y. Shao, Y. Yuan, J. Huang, Solvent annealing of perovskite-induced crystal growth for photovoltaic-device efficiency enhancement, Adv. Mater. 26 (37) (2014) 6503–6509. http://dx.doi.org/10.1002/adma.201401685.
[91] F. Di Giacomo, S. Razza, F. Matteocci, A. D'Epifanio, S. Licoccia, T.M. Brown, A. Di Carlo, High efficiency $CH_3NH_3PbI_{(3-x)}Cl_x$ perovskite solar cells with poly(3-hexylthiophene) hole transport layer, J. Power Sources 251 (2014) 152–156. http://dx.doi.org/10.1016/j.jpowsour.2013.11.053.
[92] S.T. Williams, F. Zuo, C.-C. Chueh, C.-Y. Liao, P.-W. Liang, A.K.-Y. Jen, Role of chloride in the morphological evolution of organo-lead halide perovskite thin films, ACS Nano 8 (10) (2014) 10640–10654. http://dx.doi.org/10.1021/nn5041922.
[93] M.H. Du, Efficient carrier transport in halide perovskites: theoretical perspectives, J. Mater. Chem. A 2 (2014) 9091–9098. http://dx.doi.org/10.1039/C4TA01198H.
[94] E. Mosconi, E. Ronca, F. De Angelis, First-principles investigation of the TiO_2/organohalide perovskites interface: the role of interfacial chlorine, J. Phys. Chem. Lett. 5 (2014) 2619–2625. http://dx.doi.org/10.1021/jz501127k.
[95] J. Seo, S. Park, Y.Ch Kim, N.J. Jeon, J.H. Noh, S.C. Yoon, S.I. Seok, Benefits of very thin PCBM and LiF layer for solution-processed P-I-N perovskite solar cells, Energy Environ. Sci. 7 (8) (2014) 2642–2646. http://dx.doi.org/10.1039/C4EE01216J.
[96] J.D. Gale, A.L. Rohl, The general utility lattice program (GULP), Mol. Simul. 29 (2003) 291–341. http://dx.doi.org/10.1080/0892702031000104887.
[97] D.O. Scanlon, ChW. Dunnill, J. Buckeridge, S.A. Shevlin, A.J. Logsdail, S.M. Woodley, R.A. Catlow, M.J. Powell, R.G. Palgrave, I.P. Parkin, G.W. Watson, Th.W. Keal, P. Sherwood, A. Walsh, A.A. Sokol, Band alignment of rutile and anatase TiO2, Nat. Mater. 12 (2013) 798–801. http://dx.doi.org/10.1038/nmat3697.
[98] A. Walsh, K.T. Butler, Prediction of electron energies in metal oxides, Acc. Chem. Res. 47 (2014) 364–372. http://dx.doi.org/10.1021/ar400115x.
[99] R. Brivio, AB Walker, A. Walsh, Structural and electronic properties of hybrid perovskites for high-efficiency thin-film photovoltaics from first-principles, APL Mater. 1 (4) (2013) 042111. http://dx.doi.org/10.1063/1.4824147.
[100] F. Brivio, K.T. Butler, A. Walsh, M. van Schilfgaarde, Relativistic quasiparticle self-consistent electronic structure of hybrid halide perovskite photovoltaic absorbers, Phys. Rev. B: Condens. Matter Mater. Phys. 89 (2014) 155204. http://dx.doi.org/10.1103/PhysRevB.89.155204.
[101] I. Bordello, G. Cantele, D. Ninno, Ab initio investigation of hybrid organic-inorganic perovskites based on tin halides, Phys. Rev. B 77 (2008) 235214. http://dx.doi.org/10.1103/PhysRevB.77.235214.
[102] W.J. Yin, Y.L. Wu, S.H. Wei, R. Noun, M.M. Al-Jassim, Y.F. Yan, Engineering grain boundaries in Cu_2 $ZnSnSe_4$ for better cell performance: a first-principle study, Adv. Energy Mater. 4 (2014) 1300712. http://dx.doi.org/10.1002/aenm.201300712.
[103] E. Mosconi, A. Amat, Md.K. Nazeeruddin, M. Grätzel, F. De Angelis, First-principles modeling of mixed halide organometal perovskites for photovoltaic applications, Phys. Chem. C 117 (27) (2013) 13902–13913. http://dx.doi.org/10.1021/jp4048659.
[104] S. Colella, E. Mosconi, P. Fedeli, A. Listorti, F. Gazza, F. Orlandi, P. Ferro, T. Besagni, A. Rizzo, G. Calestani, G. Gigli, F. De Angelis, R. Mosca, $MAPbI_{3-x}Cl_x$ mixed halide perovskite for hybrid solar cells: the role of chloride as dopant on the transport and structural properties, Chem. Mater. 25 (2013) 4613–4618. http://dx.doi.org/10.1021/cm402919x.
[105] V. Roiati, E. Mosconi, A. Listorti, S. Colella, G. Gigli, F. De Angelis, Stark effect in perovskite/TiO_2 solar cells: evidence of local interfacial order, Nano Lett. 14 (2014) 2168–2174. http://dx.doi.org/10.1021/nl500544c.
[106] C Quarti, G. Grancini, E. Mosconi, P. Bruno, J.M. Ball, M.M. Lee, H.J. Snaith, A. Petrozza, F. De Angelis, The Raman spectrum of the $H_3NH_3PbI_3$ hybrid perovskite: interplay of theory and experiment, Phys. Chem. Lett. 5 (2014) 279–284. http://dx.doi.org/10.1021/jz402589q.
[107] P. Umari, E. Mosconi, F. De Angelis, Relativistic GW calculations on $CH_3NH_3PbI_3$ and $CH_3NH_3SnI_3$ perovskites for solar cell applications, Sci. Rep. 4 (2014) 4467. http://dx.doi.org/10.1038/srep04467.
[108] F. De Angelis, Ace. Chem. Res. (2014) [http://dx.doi.org/10.102,l/ar500089n Article ASAP].
[109] A. Amat, E. Mosconi, E. Ronca, C Quarti, P. Umari, M.K. Nazeeruddin, M. Gratzel, F. De Angelis, Cation-induced band-gap tuning in organohalide perovskites: interplay of spin-orbit coupling and octahedra tilting, Nano Lett. 14 (2014) 3608–3616. http://dx.doi.org/10.1021/nl5012992.
[110] R. Gottesman, E. Haltzi, L. Gouda, S. Tirosh, Y. Bouhadana, A. Zaban, E. Mosconi, F. De Angelis, Extremely slow photoconductivity response of $CH_3NH_3PbI_3$ perovskites suggesting structural changes under working conditions, Phys. Chem. Lett. 5 (2014) 2662–2669. http://dx.doi.org/10.1021/jz501373f.
[111] J. Even, L. Pedesseau, C Katan, Analysis of multivalley and multibandgap absorption and enhancement of free carriers related to exciton screening in hybrid perovskites, Phys. Chem. C 118 (2014) 11566–11572. http://dx.doi.org/10.1021/jp503337a.
[112] J. Even, L. Pedesseau, J.-M. Jancu, C Katan, Importance of spin–orbit coupling in hybrid organic/inorganic perovskites for photovoltaic applications, Phys. Chem. Lett. 4 (2013) 2999–3005. http://dx.doi.org/10.1021/jz401532q.
[113] J. Even, L. Pedesseau, J.-M. Jancu, C. Katan, DFT and k · p modelling of the phase transitions of lead and tin halide perovskites for photovoltaic cells, Phys. Status Solidi RRL 8 (1) (2014) 31–35. http://dx.doi.org/10.1002/pssr.201308183.
[114] J. Even, L. Pedesseau, C. Katan, Understanding quantum confinement of charge carriers in layered 2D hybrid perovskites, ChemPhysChem. 15 (17) (2014) 3733–3741. http://dx.doi.org/10.1002/cphc.201402428.
[115] J. Even, L. Pedesseau, E. Tea, S. Almosni, A. Rolland, C Robert, J.-M. Jancu, C Cornet, C Katan, J.-F. Guillemoles, O. Durand, Density functional theory simulations of semiconductors for photovoltaic applications: hybrid organic–inorganic perovskites and III/V heterostructures, Int. J. Photoenergy 2014 (2014) 649408. http://dx.doi.org/10.1155/2014/649408.
[116] J.M. Ball, M.M. Lee, A. Hey, H.J. Snaith, Low-temperature processed meso-superstructured to thin-film perovskite solar cells, Energy Environ. Sci. 6 (13) (2013) 1739–1743. http://dx.doi.org/10.1039/C3EE40810H.
[117] A. Baumann, K. Tvingstedt, M.C. Heiber, S. Väth, C. Momblona, H.J. Bolink, V. Dyakonov, Persistent photovoltage in methylammonium lead iodide perovskite solar cells, APL Mater. 2 (2014) 8, art. no. 081501. http://dx.doi.org/10.1063/1.4885255.
[118] B.L. Oksengendler, M.B. Marasulov, N.R. Ashurov. Fundamental'nye i prikladnye voprosy fiziki. Mezhdunarodn. konf. [Fundamental and applied problems of physics. International Conference]. Tashkent: FTI ANRUz, 2015 (In Russ.).
[119] L. Onsager, Initial Recombination of Ions, Phys. Rev. 54 (8) (1938) 554.
[120] Hummel, W. Schmidt, Rad. Res. Revs. 5 (1974) 199.
[121] J.J. Thomson, Recombination of gaseous ions, the chemical combination of gases, and monomolecular reactions, Philos. Mag. Ser. 6 47 (278) (1924) 337–378. http://dx.doi.org/10.1080/14786442408634372.
[122] V.L. Bonch-Bruevich, S.G. Kalashnikov, Fizika Poluprovodnikov [Physics of Semiconductors], Nauka, Moscow, 1977 [In Russ.].
[123] R. Resta, Macroscopic polarization in crystalline dielectrics: the geometric phase approach, Rev. Mod. Phys. 66 (3) (1994) 899–915. http://dx.doi.org/10.1103/RevModPhys.66.899.
[124] R.D. King-Smith, D. Vanderbilt, Theory of polarization of crystalline solids, Phys. Rev. B 47 (3) (1993) 1651–1654. http://dx.doi.org/10.1103/PhysRevB.47.1651.
[125] S. Dall'Olio, R. Dovesi, R. Resta, Spontaneous polarization as a Berry phase of the Hartree-Fock wave function: the case of $KNbO_3$, Phys. Rev. B 56 (16) (1997) 10105–10114. http://dx.doi.org/10.1103/PhysRevB.56.10105.
[126] I. Grinberg, D.V. West, M. Torres, G. Gou, D.M. Stein, L. Wu, G. Chen, E.M. Gallo, A.R. Akbashev, P.K. Davies, J.E. Spanier, A.M. Rappe, Perovskite oxides for visible-light-absorbing ferroelectric and photovoltaic materials, Nature 503 (2013) 509–512. http://dx.doi.org/10.1038/nature12622.
[127] S.B Zhang, S.-H. Wei, A. Zunger, H. Katayama-Yoshida, Defect physics of the $CuInSe_2$ chalcopyrite semiconductor, Phys. Rev. B 57 (1998) 9642. http://dx.doi.org/10.1103/PhysRevB.57.9642.
[128] C. Persson, A. Zunger, Anomalous grain boundary physics in polycrystalline $CuInSe_2$: the existence of a hole barrier, Phys. Rev. Lett. 91 (2003) 266401. http://dx.doi.org/10.1103/PhysRevLett.91.266401.
[129] Y. Zhao, K. Zhu, Optical bleaching of perovskite $(CH_3NH_3)PbI_3$ through room-temperature phase transformation induced by ammonia, Chem. Commun. 50 (2014) 1605–1607. http://dx.doi.org/10.1039/C3CC48522F.
[130] N. Agmon, The Grotthuss mechanism, Chem. Phys. Lett. 244 (5–6) (1995) 456–462. http://dx.doi.org/10.1016/0009-2614(95)00905-J.
[131] J. Schoonman, Organic-inorganic lead halide perovskite solar cell materials: a possible stability problem, Chem. Phys. Lett. 619 (2015) 193–195. http://dx.doi.org/10.1016/j.cplett.2014.11.063.
[132] B.L. Oksengendler, O.B. Ismailova, M.B. MarasulovI, Z. Urolov, On the degradation mechanism of functioning solar cells based on organic-inorganic perovskites, Appl. Sol. Energy 50 (4) (2014) 255–259. http://dx.doi.org/10.3103/S0003701X14040100.
[133] H.J. Snaith, A. Abate, J.M. Ball, G.E. Eperon, T. Leijtens, N.K. Noel, S.D. Stranks, J.T.-W. Wang, K. Wojciechowski, W. Zhang, Anomalous hysteresis in perovskite solar cells, Phys. Chem. Lett. 5 (2014) 1511–1515. http://dx.doi.org/10.1021/jz500113x.
[134] Dzh Zaiman, Printsipy Teorii Tverdogo Tela [Principles of Solid State Theory], Mir, Moscow, 1966 [In Russ.].
[135] J. Piprek, Semiconductor Optoelectronic Devices. Introduction to Physics and Simulations, Academic Press, Amsterdam, 2003.
[136] H.A. Alturaif, Z.A. ALOthman, J.G. Shapter, S.M. Wabaidur, Use of carbon nanotubes (CNTs) with polymers in solar cells, Molecules 19 (11) (2014) 17329–17344. http://dx.doi.org/10.3390/molecules191117329.
[137] K.W. Tan, D.T. Moore, M. Saliba, H. Sai, L.A. Estroff, T. Hanrath, H.J. Snaith, U. Thermally, Induced structural evolution and performance of mesoporous block copolymer-directed alumina perovskite solar cells, ACS Nano 8 (5) (2014) 4730–4739. http://dx.doi.org/10.1021/nn500526t.
[138] R. Ulbricht, S.B. Lee, X. Jiang, K. Inoue, M. Zhang, Sh Fang, R.H. Baughman, A.A. Zakhidov, Transparent carbon nanotube sheets as 3-D charge collectors in organic solar cells, Sol. Energy Mater. Sol. Cells 91 (5) (2007) 416–419. http://dx.doi.org/10.1016/j.solmat.2006.10.002.
[139] A.B. Cook, J.D. Yuen, J.W. Micheli, A.G. Nasibulin, A. Zakhidov, Ambient method for the production of an ionically gated carbon nanotube common cathode in tandem organic solar cells, J. Vis. Exp. 93 (2014) e52380. http://dx.doi.org/10.3791/52380.